Chemical abundances as population tracers

Poul Erik Nissen

Department of Physics and Astronomy, University of Aarhus, DK-8000 Aarhus C, Denmark. pen@phys.au.dk

Summary. A discussion of elemental abundance ratios as tracers of stellar populations is presented. The emphasis is on F, G, and K stars, because they represent a wide range of ages and have atmospheres providing a 'fossil' record of the chemical evolution of the Galaxy.

Instrumentation and methods to determine chemical abundances in stellar atmospheres are discussed in Sect. 2. High-resolution ($R > 20\,000$) spectra are required to derive precise abundance ratios, but lower resolution spectra may be useful in connection with large statistical studies of populations. Most abundance analyses are based on homogeneous 1D model atmospheres and the assumption of local thermodynamic equilibrium (LTE), but recent works have shown that 3D non-LTE corrections can change the derived trends of abundance ratios as a function of stellar metallicity significantly. However, when comparing stars having similar effective temperatures, surface gravities and metallicities, 3D non-LTE corrections tend to cancel out. Such a differential approach is the best way to disentangle stellar populations on the basis of chemical abundances.

Abundance ratios particularly useful as population tracers are discussed in Sect. 3, including C/O, Na/Fe, Ni/Fe, Ba/Y, Eu/Ba, and α/Fe, where α is the average abundance of Mg, Si, Ca, and Ti. The nucleosynthesis of the elements involved occurs on different time-scales in stars and supernovae with different masses. This is the main reason that these abundance ratios can be used as population tracers.

The following sections deal with a discussion of populations in the Galactic disk, the bulge, and the halo. Based on abundance ratios, there is clear evidence for two main populations in the disk: an old, thick disk formed on a time-scale of $\sim 10^9$ years, and a younger, thin disk formed over a more extended period. For the bulge, interesting new abundance results have been obtained in recent years, including data from microlensed dwarfs, but it is too early to draw any robust conclusions about how and when the bulge formed. For the halo, there is evidence for the existence of two discrete populations with low and high values of α/Fe, respectively. The 'low-α' population has probably been accreted from dwarf galaxies, whereas the 'high-α' population may consist of ancient disk stars 'heated' to halo kinematics by merging satellite galaxies. Globular clusters stand out from the halo field stars by showing Na-O and Al-Mg anti-correlations; there is increasing evidence that they consist of multiple stellar populations.

1 Introduction

A population consists of a group of stars with a common origin and history. Hence, it is of high importance for studies of the formation and evolution of the Galaxy to detect and describe existing Galactic populations. This may be done by analyzing distribution functions for stars in space, kinematics, age and chemical composition. In particular, it is important to know if the main Galactic components, the disk, the bulge, and the halo, each consists of a single stellar population or if multiple populations are needed to fit data for kinematics, ages and abundance ratios of stars belonging to these components.

Whereas the original spatial and kinematical distributions of stars in a population are modified during the dynamical evolution of the Galaxy, it is generally assumed that the chemical composition of a stellar atmosphere provides a 'fossil' record of the composition of the Galaxy at the time and the place for the formation of the star. In this connection, F and G main-sequence and subgiant stars are of particular interest, because they span an age range as long as the lifetime of the Galaxy. Furthermore, they have an upper convection zone that mixes matter in the atmosphere with deeper layers, which tends to reduce abundance changes induced by diffusion or accretion processes (see discussion in Sect. 2.5). On the other hand, the convection zone is not so deep that elements produced by nuclear reactions in the stellar interior are brought up to the stellar surface. Hence, chemical abundances of F and G main-sequence and subgiant stars are expected to be good tracers of stellar populations.

Stars with spectral types different from F and G are also of importance as tracers of Galactic populations. O, B, and A stars may be used to probe the present composition of the Galaxy, but in some cases the atmospheric composition is affected by diffusion or accretion processes. K giants are very useful as a supplement to the F and G main-sequence stars, because they can be observed to greater distances. Their space density is, however, smaller than that of F and G dwarfs, and care should be taken because the atmospheric abundances of some elements, e.g. C and N, may be affected by convective dredge-up of the products of nuclear processes in the stellar interior.

The present review deals with the use of stellar abundance ratios to disentangle the various stellar populations in the Galaxy. Methods to determine chemical abundances in stellar atmospheres are discussed in Sect. 2 with emphasis on the high precision that may be obtained when analyzing stars in a limited region of the H-R diagram differentially. In Sect. 2, it is also discussed if element abundances in F and G main-sequence stars are affected by diffusion or accretion processes. Sect. 3 contains an inventory of abundance ratios that are particular useful as tracers of stellar populations, and a discussion of the nucleosynthesis of the involved elements. The following sections 4, 5, and 6 deal with populations associated with the Galactic disk, the bulge and the halo including globular clusters and satellite galaxies. Relations between

abundance ratios, kinematics and ages will be reviewed, and scenarios for the origin of the various populations will be discussed. Finally, Sect. 7 contains conclusions and some thoughts about future observing programmes related to chemical abundances as population tracers.

The present chapter focus on stars with metallicities in the range $-3.0 <$ [Fe/H] $< +0.4$, where [Fe/H] is a logarithmic measure of the ratio between the number of iron and hydrogen atoms in the star relative to the same ratio in the Sun [1]. Extremely metal-poor stars with [Fe/H] < -3.0 are discussed by Frebel & Norris (this volume). To some extent their chemical abundances are related to single supernovae (SNe) events, whereas a mixture of SNe with a mass distribution determined by the initial mass function (IMF) have produced the elements in more metal-rich stars.

2 Determination of stellar abundance ratios

2.1 Observation and reduction of stellar spectra

In order to derive precise abundance ratios, high-resolution ($R = \lambda/\Delta\lambda >$ 30 000) and high signal-to-noise ($S/N > 100$) spectra should ideally be obtained. For such spectra, it is possible to define a reliable continuum and measure equivalent widths of weak spectral lines that have high sensitivity to abundance changes and low sensitivity to broadening parameters as microturbulence and collisional damping. Thanks to the installation of efficient echelle spectrographs in connection with many large and medium-sized telescopes, a large number of high-quality optical ($3700 < \lambda < 9000\,\text{Å}$) spectra for F, G, and K stars have been obtained during the last couple of decades. The infrared spectral region is still lacking behind, but important abundance results for K giants in the Galactic bulge have been obtained with the Phoenix spectrograph on the Gemini South telescope (e.g. Meléndez et al. 2008) and with the ESO VLT cryogenic echelle spectrograph, CRIRES (Ryde et al. 2010).

Spectra with somewhat lower resolution ($R \sim 20\,000$) and $S/N \sim 50$ can also be used for determining abundance ratios, and may be obtained with multi-object spectrographs such as FLAMES at the ESO VLT. This has proven to be a very effective way of getting abundance data for stars in globular clusters (e.g. Carretta et al. 2009) and satellite galaxies (see review of Tolstoy et al. 2009). Furthermore, abundances of elements that are represented by many lines in stellar spectra, such as Fe and the α-capture elements Mg, Si, Ca, and Ti, can be obtained from medium-resolution spectra ($R \sim 5\,000 - 10\,000$). A good example is the determination of stellar abundances for the Sculptor dwarf spheroidal (dSph) galaxy by Kirby et al. (2009) with the multi-object spectrograph, DEIMOS, at the Keck II telescope.

---

[1]For two elements X and Y, $[X/Y] = \log(N_X/N_Y)_{star} - \log(N_X/N_Y)_{Sun}$, where N_X and N_Y are the number densities of the elements.

Even low-resolution ($R \sim 2\,000$) spectra are useful for statistical investigations of $[\alpha/\mathrm{Fe}]$[2] in Galactic surveys such a the Sloan Digital Sky Survey (SDSS) (Lee et al. 2011). Another large survey, the Radial Velocity Experiment (RAVE), which will deliver medium resolution spectra ($R \simeq 7\,500$) of $\sim 10^6$ stars in the near-infrared Ca II-triplet region (8410 - 8795 Å), has also the potential of supplying $[\alpha/\mathrm{Fe}]$ with a decent precision (Boeche et al. 2008). In the future, the ESA GAIA mission will make it possible to determine $[\alpha/\mathrm{Fe}]$ values for a still larger sample of stars based also on spectra in the Ca II-triplet region, but with a somewhat higher resolution, $R \simeq 11\,500$.

The reduction of raw spectral data should include background and sky subtraction, flat-field correction, extraction of spectra, and wavelength calibration. Standard IRAF[3] tasks or special software can be used. Care should be taken to perform a good flatfielding, including removal of possible interference fringes such that a reliable continuum can be defined from wavelength regions free of spectral lines. After normalization of the spectra, equivalent widths (EWs) of weak spectral lines can be measured by Gaussian fitting of the line profiles. For spectral lines having significant line wings (typically $EW > 70\,\mathrm{m\AA}$ in F and G main-sequence stars) the fitting should be performed with a Voigt profile. The continuum setting and equivalent width measurements may be done interactively with the IRAF task `splot` or can be done automatically (e.g. Sousa et al. 2007).

Instead of using equivalent widths, abundances can be determined by fitting a synthetic spectral line profile, calculated for a model atmosphere, to the observed line profile using the abundance of the element as a free parameter of the fit (see Fig. 1). For a line significantly blended by other spectral lines, this is the only way to derive a reliable abundance. Other lines have to be used to determine element abundances for the blending lines and to estimate line broadening parameters associated with stellar rotation and macroturbulence. Hence, the fitting is an iterative process that involves several line regions. It can be done automatically and may include a determination of the basic atmospheric parameters, effective temperature T_{eff}, and surface gravity g, from ratios between selected lines. A good example of an automatic method is presented by Barklem et al. (2005), who determine abundances of 22 elements from ESO VLT/UVES spectra by fitting hundreds of spectral windows containing suitable lines. The procedure includes the identification of continuum points in the windows, adjustments of line centers, rejection of lines disturbed by cosmic-ray hits and χ-square minimization of the difference between the synthetic and the observed spectrum. For low- and medium-resolution spectra, for which individual lines are not resolved and the continuum is not

---

[2]Throughout this chapter, α refers to the average abundance of Mg, Si, Ca, and Ti, i.e. $[\alpha/\mathrm{Fe}] = \frac{1}{4}\,([\mathrm{Mg/Fe}] + [\mathrm{Si/Fe}] + [\mathrm{Ca/Fe}] + [\mathrm{Ti/Fe}])$

[3]IRAF is distributed by the National Optical Astronomy Observatories, which are operated by the Association of Universities for Research in Astronomy, Inc., under cooperative agreement with the National Science Foundation.
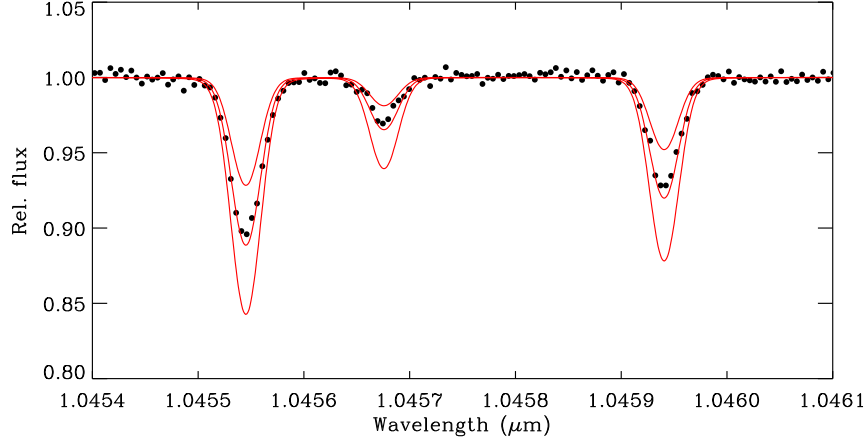
Fig. 1. The ESO/VLT CRIRES spectrum of the turnoff halo star G 29-23 ([Fe/H] = −1.7) around the near-IR, 1.046 μm S I triplet (dots) compared with synthetic LTE model-atmosphere profiles for three sulphur abundances, corresponding to [S/Fe] = 0.0, 0.3 and 0.6, respectively. As seen, the [S/Fe] = 0.3 case provides a close fit to the observations. The average S abundance determined from the three lines corresponds to [S/Fe] = 0.27 (Nissen et al. 2007).

reached, abundances can be determined by similar methods (e.g. Lee et al. 2011; Kirby et al. 2009), or may be based on line-indices that can be calibrated via high-resolution data or by model-atmosphere calculations.

2.2 Model atmospheres

Stellar abundances are normally based on a model-atmosphere analysis of the available spectra. In most cases, a plane-parallel, homogeneous (1D) model is adopted, and it is assumed that the distributions of atoms over the possible excitation and ionization states are given by Boltzmann's and Saha's equations. This condition is called 'Local Thermodynamic Equilibrium' (LTE). The temperature structure of the model is derived from the requirement that the total flux of energy as transported by radiation and convection should be constant throughout the atmosphere and given by

$$F = \sigma \, T_{\text{eff}}^4, \tag{1}$$

where σ is the Stefan-Boltzmann constant, and T_{eff} is the effective temperature of the star. Furthermore, the atmosphere is assumed to be in hydrostatic equilibrium and the pressure P as a function of optical depth τ is determined from the equation

$$\frac{dP}{d\tau} = \frac{g}{\kappa_c(T, P_e)}, \tag{2}$$

where g is the gravity in the stellar atmosphere and κ_c the continuous absorption coefficient as determined primarily by H^- absorption in optical and infrared spectra of F, G, and K stars. For these cool stars, electrons in the stellar atmosphere mainly come from the ionization of elements like Mg, Si, and Fe and the relation between total pressure and electron pressure P_e therefore depends on both metallicity and the α/Fe ratio.

Details of the construction of 1D stellar models may be found in textbooks on stellar atmospheres. The most used grid of models are the ATLAS9 models of Kurucz (1993) and the Uppsala MARCS models (Gustafsson et al. 2008). In both sets of models, convection is treated in the classical mixing-length approximation.

As reviewed by Asplund (2005), 1D models give only a first approximation to the temperature structures of stellar atmospheres. The convection creates an inhomogeneous structure with hot rising granules and cool downflows. Inhomogeneous (3D) models can be constructed by solving the standard equations for conservation of mass, momentum and energy in connection with the radiative transfer equation for a representative volume of the stellar atmosphere. The mean temperature structure of such 3D models may differ significantly from that of 1D models especially in the case of metal-poor stars. Due to the expansion of rising granulation elements and the lack of radiative heating when the line absorption coefficient is small, the 3D models have much lower temperature and electron pressure in the upper layers than classical 1D models in radiative equilibrium.

2.3 Abundance analysis

For a given model atmosphere, the flux F_λ in an absorption line can be calculated by solving the transfer equation. Integration over the line profile relative to the continuum flux F_c then gives the equivalent width

$$EW = \int \frac{F_c - F_\lambda}{F_c} d\lambda. \tag{3}$$

It is the ratio between the line and continuous absorption coefficients, κ_l/κ_c, that determines the line depth and hence the equivalent width. For a weak (un-saturated) line, the equivalent width is approximately proportional to the abundance ratio N_X/N_H, where X is the element corresponding to the line. For saturated lines, the equivalent width also depends on line broadening due to small scale turbulent gas motions. In 1D modelling this introduces an additional atmospheric parameter, the microturbulence, that can be determined from the requirement that the same Fe abundance should be derived from weak and medium-strong Fe I lines. Strong lines with damping wings are sensitive to the the value of the collisional damping constant. Clearly, the most accurate abundances are derived from weak lines if observed with high resolution and S/N.

The equivalent width of a line also depends on the oscillator strength and the populations of the energy levels corresponding to the line. In LTE, Boltzmann's and Saha's equations are used to determine the population numbers. This may, however, be a poor approximation as reviewed by Asplund (2005). Instead, one can use that a stellar atmosphere is in a steady state, i.e that the population n_i of a level i does not vary in time. This can be expressed as

$$n_i \sum_{j=1}^{N} (R_{ij} + C_{ij}) = \sum_{j=1}^{N} n_j (R_{ji} + C_{ji}), \tag{4}$$

where R and C are the transition rates for radiative and collisional processes, respectively. The summation is extended over all N levels with $j \neq i$. In such, so-called non-LTE calculations, the population numbers are found by solving N equations of the same type as Eq. (4). In addition, the transfer equation must be solved, because the radiative transition rates depend on the mean intensity of the radiation.

Departures from LTE can be large and affect derived stellar abundances very significantly (Asplund 2005). However, in some cases collisional transition rates are not well known, and the calculated non-LTE populations become rather uncertain. In particular, this is the case for inelastic collisions with neutral hydrogen atoms. Often, the recipes of Drawin (1969) are adopted, but since these estimates are based on classical physics, they only provide an order-of-magnitude estimate of the collisional rates. Hence, a scaling factor S_H to the Drawin formula has to be introduced. It may be calibrated on the basis of solar spectra by requesting that lines with different excitation potential and from different ionization stages should provide the same abundance or one may vary S_H to investigate how the uncertainty of collisional rates affects the derived abundances.

Given that non-LTE calculations are sometimes uncertain and that a grid of 3D models is not yet available, a *differential* 1D LTE analysis is often applied to determine abundance ratios. For narrow ranges in the basic atmospheric parameters, say $\pm 400 \, \mathrm{K}$ in T_{eff}, $\pm 0.4 \, \mathrm{dex}$ in $\log g$, and $\pm 0.5 \, \mathrm{dex}$ in [Fe/H], one may assume that non-LTE and 3D effects on the abundances are about the same for all stars. Hence, precise differential abundances with respect to a standard star can be derived in LTE.

For F and G stars with metallicities around [Fe/H] = 0, the Sun is an obvious choice as a standard, and logarithmic abundance ratios with respect to the Sun, like [Mg/Fe], can be derived from the same lines in the spectra of the stars and the Sun. At lower metallicities, bright stars with well known atmospheric parameters can be chosen as standards. This method has the additional advantage that the oscillator strength of a line cancels out so that its error plays no role. Such differential abundance ratios can be determined to a precision of about $\pm 0.03 \, \mathrm{dex}$ (e.g. Neves et al. 2009; Nissen & Schuster 2010). When using chemical abundances to trace stellar population, it is just these very precise differential abundance ratios at a given metallicity that are

needed. Trends of abundance ratios as a function of [Fe/H] derived under the LTE assumption are, on the other hand, less accurate, because non-LTE and 3D effects change with metallicity.

2.4 Determination of atmospheric parameters for F, G, and K stars

In order to determine precise abundance ratios, reliable values of the stellar atmospheric parameters, T_{eff}, g, and [Fe/H], must be determined. Some abundance ratios like [Mg/Fe] determined from neutral atomic lines are fairly insensitive to errors in the atmospheric parameters, but other ratios like [O/Fe] with the oxygen abundance determined from the high excitation O I triplet or from OH lines depend critically on the adopted values for T_{eff} and g.

The effective temperature of a late-type star can be determined from a colour index, e.g. $V - K$, calibrated in terms of T_{eff} by the infrared flux method. Two recent implementations of this method (González Hernández & Bonifacio 2009; Casagrande et al. 2010) give consistent calibrations of $V - K$. In the case of nearby stars for which colours are not affected by interstellar reddening, T_{eff} can be determined to an accuracy of the order of $\pm 50\,\mathrm{K}$. For more distant stars, the reddening is, however, a problem and T_{eff} is better determined spectroscopically, e.g. from the wings of Balmer lines or from the requirement that [Fe/H] derived from Fe I lines should be independent of the excitation potential of the lines. In this way, differential values of T_{eff} can be determined to a precision of $\pm 25\,\mathrm{K}$ (Nissen 2008).

The best way to determine the stellar surface gravity

$$g = G\frac{\mathcal{M}}{R^2} \tag{5}$$

is to estimate the mass $\mathcal{M}$ from stellar evolutionary tracks and the radius R from the basic relation $L \propto R^2\,T_{\mathrm{eff}}^4$, where L is the luminosity of the star. This leads to the following expression for the gravity of a star relative to that of the Sun ($\log g_{\odot} = 4.44$ in the cgs system)

$$\log \frac{g}{g_{\odot}} = \log \frac{\mathcal{M}}{\mathcal{M}_{\odot}} + 4\log \frac{T_{\mathrm{eff}}}{T_{\mathrm{eff},\odot}} + 0.4(M_{\mathrm{bol}} - M_{\mathrm{bol},\odot}), \tag{6}$$

where M_{bol} is the absolute bolometric magnitude, which can be determined from the apparent magnitude if the distance to the star is known.

This method of determining surface gravities works well for nearby stars for which distances are accurately known from Hipparcos parallaxes. For more distant late-type stars, the gravity can be determined spectroscopically from the difference in [Fe/H] derived from neutral and ionized iron lines. Fe I lines change very little with g, whereas Fe II lines change significantly. Departures from LTE in the ionization equilibrium of Fe should, however,

be taken into account. This may be done by requiring that the difference [Fe/H](Fe II) − [Fe/H](Fe I) has the same value as in the case of a standard star with a surface gravity that is accurately determined from Eq. (6). In this way differential values of $\log g$ can be determined to a precision of about ±0.05 dex (Nissen 2008).

Due to the non-LTE effects on the ionization balance of Fe, [Fe/H] should be determined from Fe II lines, because they represent the dominating ionization stage of iron. If LTE is assumed, [Fe/H] derived from Fe I lines turns out to be 0.1 to 0.2 dex lower than [Fe/H] derived from Fe II lines in the case of metal-poor F, G, and K stars. It is likely that this problem is due to a higher degree of Fe I ionization than predicted by the Saha equation (Mashonkina et al. 2011).

2.5 Diffusion and dust-gas separation of elements

As mentioned in Sect. 1, it is generally assumed that the atmosphere of a late-type star with an upper convection zone has retained a 'fossil' record of the composition of the Galaxy at the time and the place for the formation of the star. A high-resolution study of the metal-poor ([Fe/H] ~ -2) globular cluster NGC 6397 by Korn et al. (2007) indicates, however, that the abundances of Mg, Ca, Ti, and Fe in main-sequence turnoff stars are about 0.12 dex (30 %) lower than the abundances of these elements in K giants. This may be explained by downward diffusion of the elements at the bottom of the convection zone for turnoff stars. The elements are depleted by about the same factor, so the effect of diffusion on abundance ratios is less than 0.05 dex.

For the solar atmosphere, the depletion by diffusion of elements heavier than boron is predicted to have been about 0.04 dex (Turcotte & Wimmer-Schweingruber 2002) and the effect of diffusion on abundance ratios is negligible. This is confirmed by the good agreement of abundance ratios for non-volatile elements in the solar atmosphere and in the most primitive meteorites, the carbonaceous chondrites (Asplund et al. 2009). A very precise study of solar 'twin' stars (i.e. stars having nearly the same T_{eff}, g, and [Fe/H] as the Sun) by Meléndez et al. (2009) shows, on the other hand, that the Sun has a higher abundance ratio of volatile elements (C, N, O, S, and Zn) with respect to Fe than the large majority of twin stars. The deviation is about 0.05 dex. As suggested by the authors, this may be explained by selective accretion of refractory elements, including iron, on dust particles in the proto-solar disk. Thus, some fraction of the refractory elements may end up in terrestrial planets. If true, abundance ratios like [O/Fe] and [S/Fe] can deviate by ~ 0.05 dex from the original ratio in the interstellar cloud that formed the star depending on whether the star is with or without terrestrial planets.

It is concluded that the effects of diffusion may change some abundance ratios by up to 0.05 dex for metal-poor stars with relatively thin convection zones. In the case of disk stars, the abundances of volatile elements relative

to iron could be affected by dust-gas separation in connection with star and planet formation by ~ 0.05 dex. For refractory elements there are no indications of differences in abundance rations between stars with and without detected planets (Neves et al. 2009).

3 Elements used as stellar population tracers

This section presents a discussion of some abundance ratios that have been used as tracers of stellar populations. In several cases, the nucleosynthesis and chemical evolution of the corresponding elements are not well understood; nevertheless, the abundance ratios have proven to be very useful in disentangling stellar populations. In addition, the observed differences and trends provide important constraints on SNe modeling and theories of Galactic chemical evolution.

3.1 Carbon and oxygen

Abundances of C and O can be determined from spectral lines corresponding to forbidden transitions between low excitation states and allowed transitions between high-excitation states for neutral atoms. In addition, molecular CH and OH lines in the blue-UV and infrared spectral regions can be applied.

The most reliable C and O abundances are derived from the forbidden [C I] $\lambda 8727$ and [O I] $\lambda 6300$ lines, provided that these rather weak lines are measured with sufficient spectral resolution and S/N. Both lines are blended; [O I] by a Ni I line and [C I] by a weak Fe I line. These blends must be taken into account when deriving abundances. A strong collisional coupling with the ground states ensures that the [C I] and [O I] lines are formed in LTE. The correction for 3D effects is small for the Sun (Asplund 2005) but increases with decreasing metallicity and may reach as much as -0.2 dex in turnoff stars with [Fe/H] $= -2$ (Nissen et al. 2002).

The [C I] line is too weak to be a useful abundance indicator for metal-poor ([Fe/H] < -1) dwarf and subgiant stars. In giants, carbon abundances are changed by dredge-up of gas affected by CN-cycle hydrogen burning. The [O I] line, on the other hand, can be used to derive oxygen abundances in dwarfs and subgiants down to [Fe/H] ~ -2 and in giants down to metallicities around -3. Alternatively, carbon and oxygen abundances in halo stars can be derived from high-excitation atomic lines (the C I lines around 9100 Å and the O I triplet at 7774 Å) but in both cases the non-LTE effects are uncertain (Fabbian et al. 2009). CH and OH lines can be used to derive carbon and oxygen abundances even at extremely low metallicities, but they are very sensitive to $T_{\rm eff}$ and large 3D corrections should be applied (Asplund 2005). Due to these problems, C and O abundances in halo stars are quite uncertain. Carbon seems to follow iron, i.e. [C/Fe] $\simeq 0$ from [Fe/H] $= 0$ to -3 (Bensby & Feltzing 2006; Fabbian et al. 2009). [O/Fe] raises from zero to

about $+0.5\,$dex, when the metallicity of disk stars decreases from $[\text{Fe/H}]=0$ to -1 and then stays approximately constant at $[\text{O/Fe}] \simeq +0.5$ down to $[\text{Fe/H}] \simeq -2$ (Nissen et al. 2002). According to Cayrel et al. (2004), who derived oxygen abundances in giants from the [O I] line, the constant level of $[\text{O/Fe}]$ continues all the way down to $[\text{Fe/H}] \simeq -3.5$, if one assumes that 3D corrections are the same as in metal-poor dwarf stars.

Although the trends of $[\text{C/Fe}]$ and $[\text{O/Fe}]$ as a function of $[\text{Fe/H}]$ are somewhat uncertain due to non-LTE and 3D effects, the ratio between the abundances of C and O is more immune to these problems. This stems from the fact that the forbidden [C I] and [O I] lines have about the same dependence of temperature and pressure. Hence, the derived $[\text{C/O}]$ is insensitive to 3D effects. The same is the case for $[\text{C/O}]$ derived from high-excitation atomic lines. Furthermore, as shown by Fabbian et al. (2009), the non-LTE corrections of C and O abundances derived from C I and O I lines tend to cancel, so that the trend of $[\text{C/O}]$ vs. $[\text{O/H}]$ is fairly independent of the choice of the hydrogen collision parameter, S_{H} (see Sect. 2.3). Fig. 2 shows this trend for $S_{\text{H}} = 1$, with the abundances determined from forbidden lines for disk stars and from high-excitation atomic lines for the halo stars.
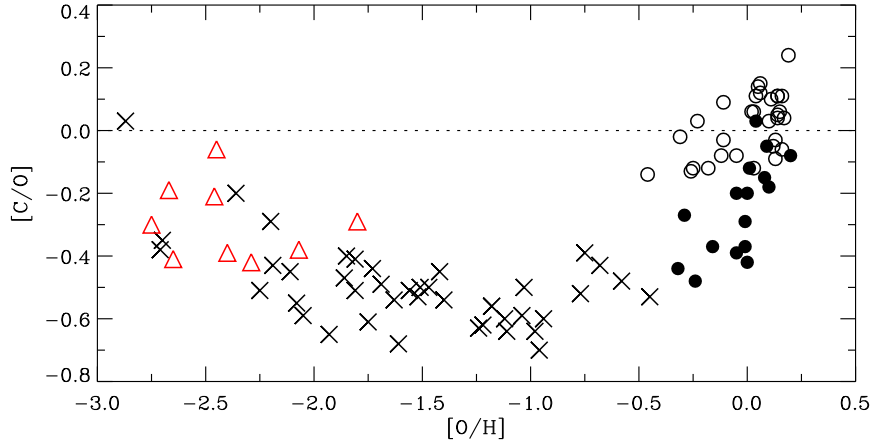
Fig. 2. The carbon-to-oxygen ratio as a function of the oxygen abundance. Open circles refer to thin-disk and filled circles to thick-disk stars with data adopted from Bensby & Feltzing (2006). Crosses are halo stars from Fabbian et al. (2009), and (red) triangles show DLA data from Cooke et al. (2011).

Carbon is synthesized in stellar interiors by the triple-α process, but it is unclear which objects are the main contributors to the chemical evolution of carbon in the Galaxy. Type II SNe, Wolf-Rayet stars, intermediate- and low-mass stars in the planetary nebula phase, and stars at the end of the giant phase have been suggested. Oxygen, on the other hand, seem to be

produced exclusively by α-capture on C in short-lived massive stars and is dispersed to the interstellar medium by type II SNe. Hence, the C/O ratio has the potential of being a good tracer of stellar populations. The separation between thin- and thick-disk stars in Fig. 2 shows that this is indeed the case.

The approximately constant $[C/O] \simeq -0.5$ for halo stars with $[O/H]$ between -2.0 and -0.5 probably corresponds to the C/O yield ratio for massive stars. The increase in $[C/O]$ for the thick-disk stars may be due to metallicity dependent winds from Wolf-Rayet stars, whereas the delayed production of carbon by low- and intermediate-mass stars can explain the higher $[C/O]$ in thin-disk stars. The upturn of $[C/O]$ at the lowest values of $[O/H]$, which is also found for distant damped Lyman-α (DLA) galaxies (Cooke et al. 2011), could be due to enhanced carbon production by massive first generation stars with extremely high rotation velocities (Chiappini et al. 2006).

3.2 Intermediate-mass elements

The even-Z elements, Mg, Si, S, Ca, and Ti are mainly produced by successive capture of α-particles in connection with carbon, oxygen and neon burning in massive stars and dispersed into the interstellar medium by type II supernovae explosions on a time-scale of $\sim 10^7$ years. Iron is also produced by SNe II, but the bulk of Fe comes from type Ia SNe on a much longer time-scale ($\sim 10^9$ years). Hence, the ratio between the abundance of an α-capture element and iron in a star depends on how long the star-formation process had proceeded before the star was formed. In this way, $[\alpha/Fe]$ becomes an important tracer of populations.

Mg, Si, Ca, and Ti abundances can be determined from several weak atomic lines in the optical spectra of late-type stars, whereas sulphur is more difficult as discussed below. Traditionally, $[\alpha/Fe]$ is therefore defined as the average value of $[Mg/Fe]$, $[Si/Fe]$, $[Ca/Fe]$, and $[Ti/Fe]$ (see Sect. 2.1). As discussed by Asplund (2005), departures from LTE have some effects on the metallicity trends of $[\alpha/Fe]$ but probably not more than 0.1 dex, when weak lines are used. If the abundances are based on neutral lines, $[\alpha/Fe]$ is quite insensitive to $T_{\rm eff}$ and 3D effects, although high excitation lines are to be preferred (Asplund 2005, Fig. 8)

The trend of $[\alpha/Fe]$ with metallicity is characterized by an increase of about 0.3 dex when $[Fe/H]$ decreases from 0 to -1. Below $[Fe/H] = -1$, $[\alpha/Fe]$ is distributed around a plateau at 0.3 dex, but as discussed later, there are very significant differences in $[\alpha/Fe]$ at a given metallicity related to stellar populations both for disk and halo stars.

Sulphur is an α-capture element, and $[S/Fe]$ is therefore expected to show a plateau-like behaviour for halo stars, but very high values $[S/Fe] \sim 0.8$ have been claimed at the lowest metallicities (Israelian & Rebolo 2001). These values may, however, be spurious due to the difficulty of measuring the very weak S I line at 8694.6 Å. On the basis of stronger S I lines at 9212.9 and 9237.5 Å measured with UVES and corrected for telluric absorption lines,

Nissen et al. (2007) find a plateau-like behaviour of [S/Fe] as shown in Fig. 3. Non-LTE corrections from Takeda et al. (2005) corresponding to $S_{\mathrm{H}} = 1$ were included for sulphur, and the iron abundances were derived from Fe II lines with negligible non-LTE effects (Mashonkina et al. 2011) . This result is supported by CRIRES observations of the near-IR S I triplet (see Fig. 1). Further studies of sulphur in Galactic stars would be important, especially because S is a volatile element that is undepleted onto dust. As such it can be used to measure the α-enhancement of DLA galaxies.
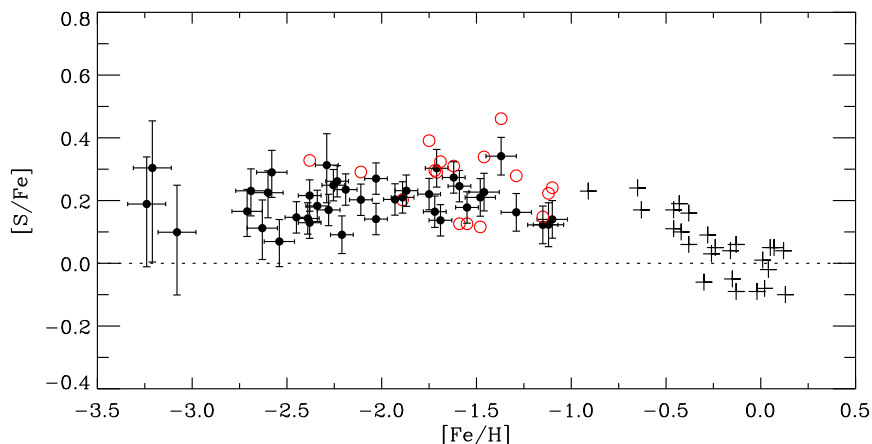
Fig. 3. [S/Fe] as a function of [Fe/H]. Plus signs refer to data for disk stars from Chen et al. (2002) and circles to halo stars from Nissen et al. (2007). Filled circles with error bars are based on S abundances derived from the $\lambda\lambda9212.9, 9237.5$ S I lines, whereas open (red) circles show data determined from the weak $\lambda8694.6$ S I line.

In addition to the α-capture elements, Na is an interesting and sensitive tracer of stellar populations. It is thought to be made during carbon and neon burning in massive stars and is expelled by type II SNe together with the α-elements. The amount of Na made is, however, controlled by the neutron excess, which depends on the initial heavy element abundance in the star (Arnett 1971). This is probably the explanation of the fact that [Na/Mg] in halo stars correlates with [Mg/H] with a slope of about 0.5 (Nissen & Schuster 1997; Gehren et al. 2004).

Na abundances are best determined from the relatively weak Na I doublets $\lambda\lambda5682.6, 5688.2$ and $\lambda\lambda6154.2, 6160.7$, for which non-LTE and 3D corrections are rather small (Asplund 2005). At low metallicities, [Fe/H] < -2.0, these lines are too faint to be measured, and Na abundances are derived from the Na I D $\lambda\lambda5890.0, 5895.9$ resonance lines. For this doublet, the non-LTE correction is large and reaches -0.4 dex for extremely metal-poor stars (Gehren

et al. 2004). Furthermore, the use of these lines is sometimes complicated by overlapping interstellar Na I D lines and telluric H_2O lines.

In addition to Na production in massive stars, sodium can also be made in hydrogen-burning shells of intermediate- and low-mass stars via the CNO and Ne-Na cycles. This is probably the explanation of the Na-O anti-correlation in globular clusters as further discussed in Sect. 6.3.

3.3 The iron-peak elements

Among the iron-peak elements - Cr to Zn - the even-Z elements Cr, Fe, and Ni are represented by many lines in the spectra of late-type stars, which makes it possible to determine very precise abundance ratios, [Cr/Fe] and [Ni/Fe].

The ratio between Cr and Fe abundances is found to be the same as in the Sun, i.e. [Cr/Fe] $\simeq 0$, for all Galactic populations with [Fe/H] > -2. Below this metallicity, McWilliam et al. (1995) and Cayrel et al. (2004) have found a smooth decrease of [Cr/Fe] to ~ -0.5 at [Fe/H] $= -4$ based on an LTE study of Cr I lines in very metal-poor giants. This is surprising, because Cr and Fe are predicted to be synthesized in constant ratios by explosive silicon burning in both type II and Ia SNe. The problem seems to have been solved by Bergemann & Cescutti (2010), who find that the derived decline of [Cr/Fe] is an artifact caused by the neglect of non-LTE effects. They obtain a very satisfactory agreement between non-LTE Cr abundances derived from Cr I and Cr II lines when using surface gravities based on Hipparcos parallaxes.

For a long time, the Ni/Fe ratio was also thought to be solar in all stars. This is clearly the case for disk population stars (e.g. Chen et al. 2000), but Nissen & Schuster (1997, 2010) have shown that Ni is underabundant relative to Fe, i.e. [Ni/Fe] ~ -0.1 to -0.2, in some halo stars with [Fe/H] > -1.4. These stars have also low [α/Fe] and [Na/Fe] values, and a tight correlation between [Ni/Fe] and [Na/Fe] is present (see Sect. 6.1). Similar stars are found in dwarf galaxies (Tolstoy et al. 2009). The reason for this correlation is probably that the supernovae yields of ^{23}Na and ^{58}Ni depend on the neutron excess (see the detailed discussion by Venn et al. 2004).

The determination of abundances of the odd-Z elements Mn, Co, and Cu is more difficult than in the case of Cr, Fe, and Ni. There are fewer lines available and hyper-fine-structure (HFS) splitting has to be taken into account. Furthermore, non-LTE effects seem to be very significant. Positive corrections of both [Mn/Fe] (Bergemann & Gehren 2008) and [Co/Fe] (Bergemann et al. 2010) are obtained, although the size of these corrections depends somewhat on the adopted S_H parameter for hydrogen collisions. This means that the strong decline of [Mn/Fe] as a function of decreasing [Fe/H] found from an LTE analysis of Mn I lines by e.g. Reddy et al. (2006) and Neves et al. (2009) has to be modified to a more shallow trend. For Co the non-LTE study of Bergemann et al. (2010) leads to surprisingly large over-abundances

of cobalt with respect to iron for halo stars, a result that is in disagreement with expectations from presently calculated supernovae yields.
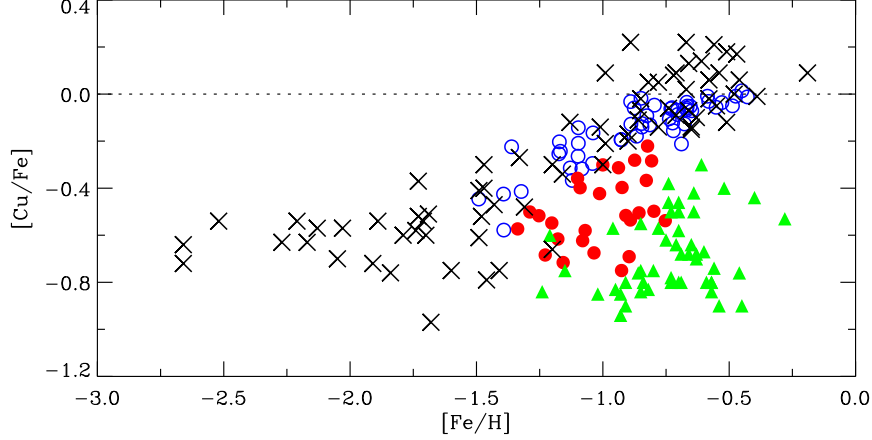
Fig. 4. [Cu/Fe] as a function of [Fe/H]. Stars studied by Mishenina et al. (2002) are indicated by crosses. Open (blue) circles refer to high-α stars and filled (red) circles to low-α halo stars from Nissen & Schuster (2011). Filled (green) triangles are data for giant stars in the inner part of the Large Magellanic Cloud adopted from Pompéia et al. (2008).

Copper is a very interesting element as a tracer of metal-poor stellar populations. Abundances can be determined from the Cu I lines at 5105.5, 5218.2 and 5782.1 Å. They are affected by HFS splitting to different degrees. Non-LTE calculations are not yet available, but LTE data show that [Cu/Fe] $\simeq 0$ for disk stars with no significant difference between the thin and the thick disk (Reddy et al. 2006). At [Fe/H] ~ -1, [Cu/Fe] starts to decline steeply and reaches a plateau of [Cu/Fe] ~ -0.6 below [Fe/H] $\simeq -1.6$ (Mishenina et al. 2002) as shown in Fig. 4. Low-α halo stars deviate, however, from this trend with a [Cu/Fe] deficiency of 0.2 to 0.5 dex (Nissen & Schuster 2011). The same is the case for the more metal-rich part of stars in the globular cluster ω Centauri (Cunha et al. 2002), and stars belonging to the Sagittarius dSph galaxy (Sbordone et al. 2007) and the Large Magellanic Cloud (Pompéia et al. 2008) as shown in Fig. 4. These [Cu/Fe] data provide important constraints on the nucleosynthesis of Cu. Romano & Matteucci (2007) suggest that copper is initially made by explosive nucleosynthesis in type II SNe and later by a metallicity dependent neutron-capture process (the weak s-process) in massive stars.

Zinc abundances can be determined from the $\lambda\lambda 4722.2, 4810.5$ Zn I lines. Non-LTE and 3D corrections are modest, i.e. of the order of $+0.1$ dex for metal-poor stars (Nissen et al. 2007). It is sometimes assumed that [Zn/Fe]

= 0, which means that Zn can be used as a proxy of Fe in determining the metallicity of interstellar gas, e.g. in DLA systems; as a volatile element Zn is not depleted onto dust like Fe. Newer studies show, however, that [Zn/Fe] reaches +0.15 dex in metal-poor disk stars with perhaps a small separation between thin- and thick-disk stars (Bensby et al. 2005). For halo stars, [Zn/Fe] increases from zero at [Fe/H] = −1 to [Zn/Fe] ≃ 0.2 at [Fe/H] = −2.5 (Nissen et al. 2007), and at still lower metallicities [Zn/Fe] increases steeply to [Zn/Fe] ≃ 0.5 at [Fe/H] = −3.5 (Cayrel et al. 2004, Nissen et al. 2007). Hence the behaviour of zinc is complicated, and the nucleosynthesis of this element is not well understood. Several ways of producing Zn have been suggested: the weak s-process in massive stars, explosive Si burning in type II and type Ia SNe, and the main s-process in low- and intermediate-mass stars.

3.4 The neutron capture elements

Among the heaviest elements, Y, Ba, and Eu are of particular interest as tracers of stellar populations. They are made by neutron capture processes, which are traditionally divided into the slow s-process and the rapid r-process. In the s-process, neutrons are added on a long time-scale compared to that of β decays so that nuclides of the β-stability valley are built up. In the r-process, neutrons are added so fast that nuclides on the neutron-rich side of the stability valley are made. The s-process is divided into the main s-process that occurs in low- and intermediate-mass asymptotic giant branch (AGB) stars and the weak s-process occurring in massive stars. The r-process is not well understood, but it is thought to occur in connection with type II SNe explosions.

The relative contribution of the s- and the r-process to heavy elements in the solar system has been determined by Arlandini et al. (1999). Barium is called an s-process element, because 81% of the solar Ba is due to the s-process. Europium, on the other hand, is an r-process element, because 94% in the Sun originates from the r-process. In metal-poor stars, for which only massive stars have contributed to the nucleosynthesis of the elements, both Ba and Eu are, however, made by the r-process, provided that the contribution from the weak s-process is negligible. In such metal-poor stars, one would expect to find an r-process ratio $N_{\mathrm{Eu}}/N_{\mathrm{Ba}} \simeq 5$ between the abundances of europium and barium corresponding to [Eu/Ba] ≃ 0.7. These considerations suggest that [Eu/Ba] may be a useful tracer of stellar populations. As seen from Fig. 5, this is confirmed by Mashonkina et al. (2003).

Ba abundances can be determined from subordinate Ba II lines at 5853.7, 6141.7, and 6496.9 Å. The stronger resonance line at 4554.0 Å may also be used, but the analysis of this line is complicated by the presence of isotopic and HFS splitting. Europium abundances are primarily obtained from the Eu II line at 4129.7 Å, which has to be analyzed by spectrum synthesis techniques, because the line is strongly broadened by isotopic and HFS splitting.
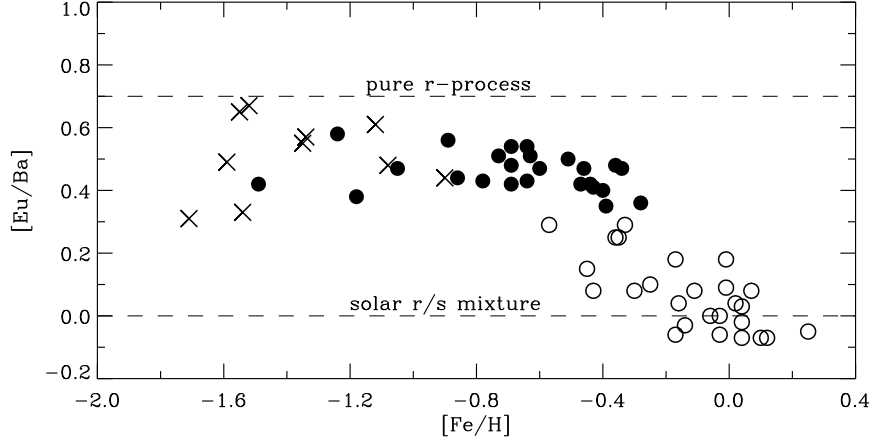
Fig. 5. [Eu/Ba] as a function of [Fe/H] with data adopted from Mashonkina et al. (2003). Crosses refer to stars with halo kinematics, filled circles to thick-disk stars and open circles to thin-disk stars.

The barium-to-yttrium ratio is another interesting tracer of stellar populations. Yttrium ($Z = 39$) belongs to the first peak of s-process elements around the neutron magic number $N = 50$, whereas barium ($Z = 56$) is at the second peak around $N = 82$. The ratio Ba/Y (sometimes called heavy-s to light-s, hs/ls) depends on the the neutron flux per seed nuclei, and is predicted to be high for metal-poor, low-mass AGB stars (Busso et al. 1999). As pointed out by Venn et al. (2004), the Ba/Y ratio in stars belonging to dSph satellite galaxies is much higher than Ba/Y in Galactic halo stars with differences on the order of 0.6 dex in the metallicity range $-2 < [\mathrm{Fe/H}] < -1$. Similar large offsets are found for stars with [Fe/H] around -1 in the globular cluster ω Cen (Smith et al. 2000) and for stars in the LMC (Pompéia et al. 2008). According to Fenner et al. (2006), this indicates that the chemical evolution of these systems has been so slow that winds from low-mass AGB stars have started to enrich the interstellar medium with s-process elements at a metallicity around $[\mathrm{Fe/H}] \sim -2$.

4 The Galactic disk

4.1 The thick and the thin disk

A long-standing problem in studies of Galactic structure and evolution has been the possible existence of a population of stars having kinematics, ages, and chemical abundances in between the characteristic values for the halo and the disk.

On the basis of a large program of $uvby$-β photometry of F and early G type main-sequence stars within 100 pc, Strömgren (1987) concluded that an *intermediate Population II* does exist. [Fe/H] was determined from a metallicity index $m_1 = (v-b)-(b-y)$, which is sensitive to the line blanketing in the v-band, and age was derived from the position of a star in the c_1 - $(b-y)$ diagram, where $c_1 = (u-v)-(v-b)$ is a measure of the Balmer discontinuity at 3650 Å and hence of the surface gravity of the star. The colour index $(b-y)$ is used as a measure of T_{eff}. After discussing the calibration of the m_1 index in terms of [Fe/H], and c_1 as a function of absolute magnitude, Strömgren found that intermediate Population II consists of 10-15 Gyr old stars having $-0.8 < $ [Fe/H] $ < -0.4$ and velocity dispersions that are significantly greater than those of the younger, more metal-rich disk stars.

In a seminal paper, Gilmore & Reid (1983) showed that the distribution of stars in the direction of the Galactic South Pole cannot be fitted by a single exponential, but requires two disk components – a *thin disk* with a scale height of 300 pc and a *thick disk* with a scale height of about 1300 pc. They identified intermediate Population II with the sum of the metal-poor end of the thin disk and the thick disk. Following this work, it has been intensively discussed if the thin and thick disks are discrete components of our Galaxy or if there is a more continuous sequence of stellar populations connecting the Galactic halo and the thin disk.

In another important paper, Edvardsson et al. (1993) derived precise abundance ratios for 189 stars belonging to the disk. Stars in the temperature range $5600 < T_{\mathrm{eff}} < 7000$ K and somewhat evolved away from the zero-age main-sequence were selected from $uvby$-β photometry of stars in the solar neighbourhood (i.e. in a region around the Sun with a radius of ~ 100 pc) and divided into nine metallicity bins ranging from [Fe/H] ~ -1.0 to $\sim +0.3$. In each metallicity bin the ~ 20 brightest stars were observed. Hence, there is no kinematical bias in the selection of the stars.

The Edvardsson et al. (1993) survey provides clear evidence for a scatter in [α/Fe] at a given metallicity for stars in the solar neighbourhood. This is shown in Fig. 6. As seen, [α/Fe] for stars in the metallicity range $-0.8 < $ [Fe/H] $ < -0.4$ is correlated with the mean galactocentric distance R_m in the stellar orbit. Stars with $R_m > 9$ kpc tend to have lower [α/Fe] than stars with $R_m < 7$ kpc, and stars belonging to the solar circle lie in between. Assuming that R_m is a statistical measure of the distance from the Galactic center at which the star was born, Edvardsson et al. explained the [α/Fe] variations

as due to a star formation rate that declines with galactocentric distance. In other words, type Ia SNe start contributing iron at a higher [Fe/H] in the inner parts of the Galaxy than in the outer parts.
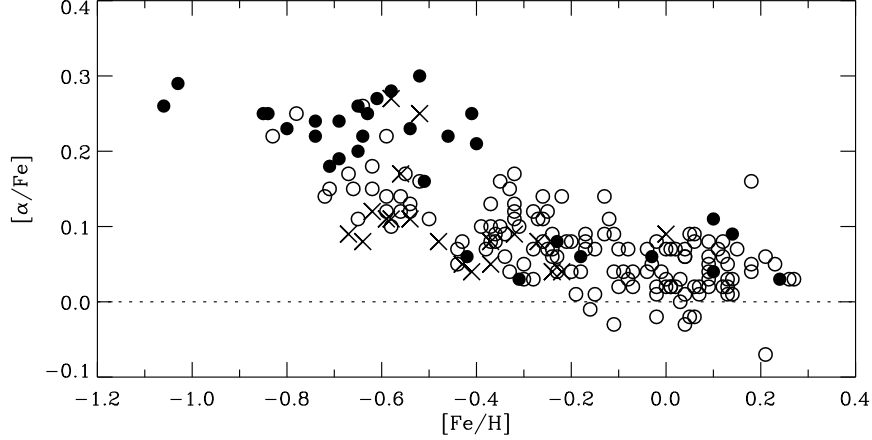
Fig. 6. $[\alpha/\mathrm{Fe}]$ as a function of [Fe/H] with data from Edvardsson et al. (1993). Stars shown with filled circles have a mean galactocentric distance in their orbits $R_m < 7$ kpc. Open circles refer to stars with $7 < R_m < 9$ kpc, and crosses refer to stars with $R_m > 9$ kpc.

The group of stars in Edvardsson et al. (1993) with $R_m < 7$ kpc have kinematical properties similar to those of the thick disk, for which the dispersions of the Galactic velocity components, U, V, and W, with respect to the Local Standard of Rest (LSR) are determined to be $(\sigma_U, \sigma_V, \sigma_W) \simeq (65, 50, 40)\,\mathrm{km\,s^{-1}}$, and for which the asymmetric drift with respect to the LSR is $V_{\mathrm{ad}} \simeq -50\,\mathrm{km\,s^{-1}}$. In comparison, thin disk stars in the solar neighbourhood have $(\sigma_U, \sigma_V, \sigma_W) \simeq (40, 30, 20)\,\mathrm{km\,s^{-1}}$ and $V_{\mathrm{ad}} \simeq -10\,\mathrm{km\,s^{-1}}$. Thus, thick-disk stars move on more eccentric orbits than the thin-disk stars, and due to the increasing density of stars towards the inner part of the Galaxy, thick disk stars presently situated in the solar neighbourhood tend to be close to the apo-galactic distance in their orbits. This means that they have smaller mean galactocentric distances than the thin-disk stars. The differences in $[\alpha/\mathrm{Fe}]$ shown in Fig. 6 may, therefore, also be interpreted as due to a systematic difference in $[\alpha/\mathrm{Fe}]$ between the thin and the thick disk. Apparently, Gratton et al. (1996) were first to suggest this interpretation of the $[\alpha/\mathrm{Fe}]$ data.

A more clear chemical separation between thin- and thick-disk stars has been obtained by Fuhrmann (2004). For a sample of nearby stars with $5300 < T_{\mathrm{eff}} < 6600\,\mathrm{K}$ and $3.7 < \log g < 4.6$, he derives very precise Mg abundances from Mg I lines and Fe abundances from Fe I and Fe II lines. In a [Mg/Fe]

vs. [Fe/H] diagram, stars with thick disk kinematics have [Mg/Fe] $\simeq +0.4$ and [Fe/H] between -1.0 and -0.3. The thin disk stars show a well-defined sequence from [Fe/H] $\simeq -0.6$ to $+0.4$ with [Mg/Fe] decreasing from $+0.2$ to 0.0. Hence, there is a [Mg/Fe] separation between thick and thin disk stars in the overlap region $-0.6 <$ [Fe/H] < -0.3 with only a few 'transition' stars. This is even more striking in a diagram, where [Fe/Mg] is plotted as a function of [Mg/H] (Fuhrmann 2004, Fig. 34).

On the basis of stellar ages derived from evolutionary tracks in the M_{bol} - $\log T_{\mathrm{eff}}$ diagram, Fuhrmann (2004) finds that the maximum age of thin disk stars is about 9 Gyr, whereas thick disk stars have ages around 13 Gyr. This suggests that the systematic difference of [Mg/Fe] is connected to a hiatus in star formation between the thick and thin disk phases.

4.2 The [α/Fe] distribution of disk stars

Two major studies of abundance ratios in thin- and thick-disk stars (Bensby et al. 2005; Reddy et al. 2003, 2006) are based on kinematically selected groups of stars in the solar neighbourhood. In these works, it is assumed that the kinematics of stars can be represented by Gaussian distribution functions for the velocity components, U, V, and W with respect to the LSR. The kinematical probability that a star belongs to a given population: thin disk, thick disk or halo (i = 1, 2, 3) is then given by

$$P_i \propto k_i\, f_i \exp\left(-\frac{U^2}{2\sigma_{U_i}^2} - \frac{(V - V_{\mathrm{ad}_i})^2}{2\sigma_{V_i}^2} - \frac{W^2}{2\sigma_{W_i}^2}\right), \qquad (7)$$

where $k = (2\pi)^{-3/2}(\sigma_U \sigma_V \sigma_W)^{-1}$ is the standard normalization constant, and f the relative number of stars in a given population. $\sigma_U, \sigma_V,$ and σ_W are the velocity dispersions in $U, V,$ and W, respectively, and V_{ad} the asymmetric drift velocity for the population. As an example, the values used by Reddy et al. (2006) are given in Table 1. Some of these values have considerable uncertainties. Depending on how the populations is defined, the fraction of thick disk stars in the solar neighbourhood may be as high as 20 % (Fuhrmann 2004), and the local fraction of halo stars is often estimated to be on the order of 0.001.

In the works of Bensby et al. (2005) and Reddy et al. (2003, 2006) precise abundance ratios for F and G dwarfs have been derived for samples of stars kinematically selected to have high probability of belonging to either the thin or the thick disk. Thus, in Reddy et al. (2006) the probability limit for each population is $P > 70\%$. The resulting [α/Fe] – [Fe/H] diagram is shown in Fig. 7. As seen, there is a gap in [α/Fe] between thin- and thick-disk stars for the metallicity range $-0.7 <$ [Fe/H] -0.4. Around [Fe/H] $= -0.3$ a few stars seem to connect the two populations like in the corresponding diagram of Fuhrmann (2004).

Table 1. Velocity dispersions, asymmetric drift and fraction of stars in the solar neighbourhood for the thin-disk, thick-disk and halo populations as adopted by Reddy et al. (2006) for calculating membership probabilities.

Population	σ_U $\mathrm{km}\,s^{-1}$	σ_V $\mathrm{km}\,s^{-1}$	σ_W $\mathrm{km}\,s^{-1}$	V_{ad} $\mathrm{km}\,s^{-1}$	f
Thin disk	43	28	17	-9	0.93
Thick disk	67	51	42	-48	0.07
Halo	131	106	85	-220	0.006
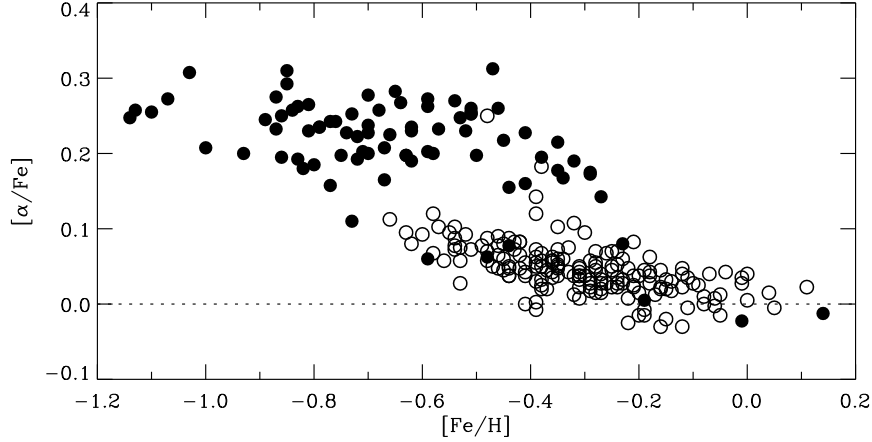
Fig. 7. $[\alpha/\mathrm{Fe}]$ as a function of $[\mathrm{Fe/H}]$ according to Reddy et al. (2003, 2006). Stars indicated by open circles have a probability $P > 70\,\%$ of belonging to the thin disk, whereas stars represented by filled circles have $P > 70\,\%$ of belonging to the thick disk.

The $[\alpha/\mathrm{Fe}]$ diagram of Bensby et al. (2005) looks similar to Fig. 7 except that their thick-disk stars continue all the way up to solar metallicity with decreasing values of $[\alpha/\mathrm{Fe}]$. Thus, Bensby et al. claim that star formation in the thick disk continued long enough to include chemical enrichment from type Ia SNe. This is, however, not so evident from the data of Reddy et al. (2006). In Fig. 7, the thick disk terminates around $[\mathrm{Fe/H}] \simeq -0.3$ with little or no decrease of $[\alpha/\mathrm{Fe}]$.

Given that the thin- and thick-disk stars of Bensby et al. (2005) and Reddy et al. (2003, 2006) have been kinematically selected, the question arises if there are stars with intermediate kinematics filling the gap in $[\alpha/\mathrm{Fe}]$ between the two populations. The problem has be addressed by Ramírez et al. (2007), who derived oxygen abundances for 523 nearby stars from a non-LTE analysis of the O I triplet at 7774 Å. A similar splitting as in Fig. 7 between stars with thin- and thick-disk kinematics is obtained, and stars

with intermediate kinematics do not fill the gap in [O/Fe]; they have either high [O/Fe] or low [O/Fe].

Another set of abundance data that can be used to study the problem of a gap in $[\alpha/\text{Fe}]$ between thin- and thick-disk stars has been obtained by Neves et al. (2009) from ESO/HARPS high-resolution spectra of 451 F, G, and K main-sequence stars in the solar neighbourhood. The main purpose of this project is to detect planets around stars by measuring radial velocity variations with a precision of $1\,\text{m}\,\text{s}^{-1}$. As a by-product, stellar abundance ratios relative to those of the Sun have been derived.

Neves et al. (2009) show that trends of abundance ratios as a function of [Fe/H] are the same for stars with and without planets. For both groups there is a bifurcation of the abundances of α-capture elements relative to iron. This is shown in Fig. 8, where only stars having T_{eff} within $\pm 300\,\text{K}$ from the effective temperature of the Sun have been included in order to obtain a very high precision of $[\alpha/\text{Fe}]$, i.e. $\sigma\,[\alpha/\text{Fe}] \simeq \pm 0.02$. At metallicities $[\text{Fe}/\text{H}] < -0.1$, there is a gap in $[\alpha/\text{Fe}]$ between 'high-α' and 'low-α' stars. Hence, the data of Neves et al. (2009) confirm the dichotomy in $[\alpha/\text{Fe}]$ found by Bensby et al. (2005) and Reddy et al. (2006). Furthermore, the data of Neves et al. support the claim of Bensby et al. (2005), that the thick disk have metallicities stretching up to solar metallicity.

The sample of stars from Neves et al. (2009) is *volume limited*; hence, the gap between high-α and low-α stars cannot be due to exclusion of stars with intermediate kinematics. Figure 8 shows the distribution of the two populations in a Toomre energy diagram. As seen, the majority of high-α stars have a total space velocity with respect to the LSR larger than $85\,\text{km s}^{-1}$, which classify them as thick-disk stars, but several high-α stars are kinematically mixed with the low-α stars. This is an example of how an abundance ratio is a more clean separator of stellar populations than kinematics.

Considering that the high-α, thick-disk stars tend to be older than the oldest of the low-α, thin-disk stars (Fuhrmann 2004; Reddy et al. 2006), the difference in $[\alpha/\text{Fe}]$ is often explained in a scenario, where a period of rapid star formation in the early Galactic disk was interrupted by a merging satellite galaxy that 'heated' the already formed stars to thick-disk kinematics. This was followed by a hiatus in star formation, in which metal-poor gas was accreted and type Ia SNe caused $[\alpha/\text{Fe}]$ to decrease. When star formation resumed, the first thin-disk stars were formed with low metallicity and low $[\alpha/\text{Fe}]$. This scenario also explains the systematic differences in [C/O] (Fig. 2) and [Eu/Ba] (Fig. 5) between thin- and thick-disk stars.

Haywood (2008) has pointed out that the low-metallicity thin-disk stars in the solar neighbourhood tend to have positive values of the V velocity component. Such stars have mean galactocentric distances larger than the distance of the Sun from the Galactic center, and hence they are likely to have been formed in the outer part of the Galactic disk. Thick-disk stars, on the other hand, have negative values of V and tend to be formed in the
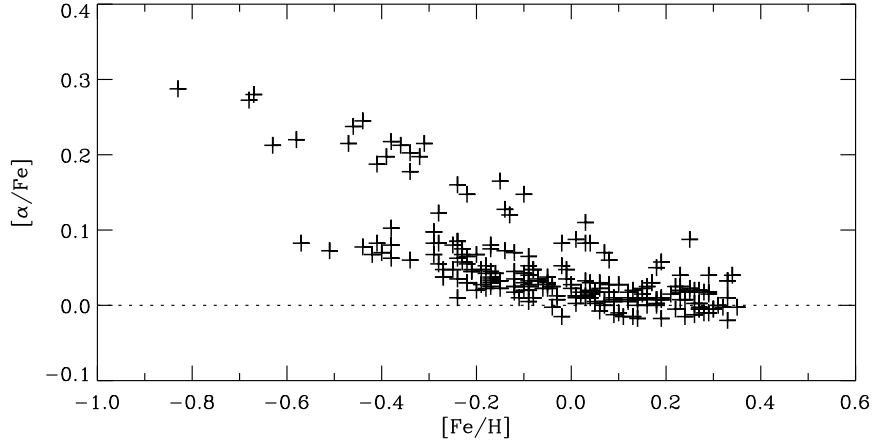
Fig. 8. The $[\alpha/\text{Fe}]$ vs. [Fe/H] distribution for a *volume limited* sample of main-sequence stars from Neves et al. (2009). Only stars with T_{eff} within $\pm 300\,\text{K}$ from the effective temperature of the Sun have been included.
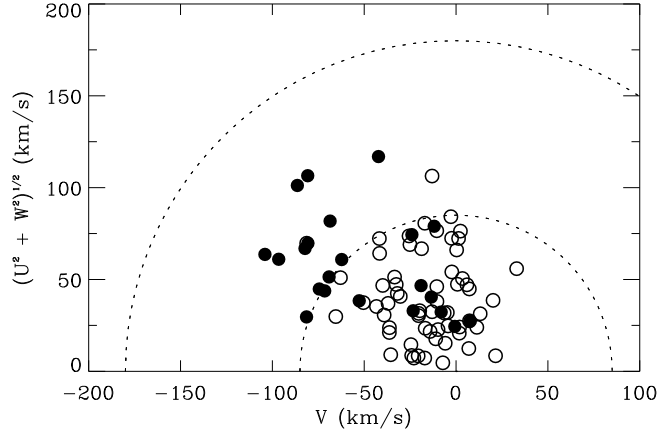
Fig. 9. The Toomre diagram for stars from Fig. 8 with [Fe/H] < -0.1. High-α stars are shown with filled circles and low-α stars with open circles. The two circles delineate constant total space velocities with respect to the LSR, $V_{\text{tot}} = 85$ and $180\,\text{km s}^{-1}$, respectively.

inner Galactic disk. From these considerations, Haywood suggests that the bimodal distribution in $[\alpha/\mathrm{Fe}]$ may be due to radial mixing of stars in the disk.

This scenario has been further investigated by Schönrich & Binney (2009a, 2009b) in a model for the chemical evolution of the Galactic disk, for which the star formation rate is monotonically decreasing, and which includes radial migration of stars and gas flows. The model successfully fit the metallicity distribution and the large scatter in the age-metallicity relation for stars in the Geneva-Copenhagen survey (Nordström et al. 2004). The model also predicts a bimodal distribution of $[\alpha/\mathrm{Fe}]$ for stars in the solar neighbourhood with the high-α stars coming from the inner parts of the Galactic disk and the low-α stars from the outer part. It will, however, be interesting to see if the model can reproduce a gap in the $[\alpha/\mathrm{Fe}]$ distribution for disk stars as found from the data of Neves et al. (2009).

4.3 Abundance gradients in the disk

In models for the chemical evolution of the Galactic disk, observed abundance gradients provide important constraints. Gradients may be determined from B-type stars and H II regions, but the most precise results have been obtained from Cepheids. These variable stars are bright enough to be studied at large distances and accurate values of the distances can be obtained from the period-luminosity relation. Earlier results suggested a steeper metallicity gradient in the inner part of the galaxy as compared to the outer part with a break in the gradient occurring around 10 kpc. According to newer work this is, however, not so obvious. For 54 Cepheids ranging in galactocentric distance R_G from 4 to about 14 kpc, Luck et al. (2006) find an overall gradient $d[\mathrm{Fe/H}]/dR_G = -0.06 \, \mathrm{dex \, kpc^{-1}}$, but there seems to be a significant cosmic scatter around a linear fit to the data. A region at Galactic longitude $l \sim 120$ degrees and a distance of 3-4 kpc from the Sun has enhanced metallicities with $\Delta\,[\mathrm{Fe/H}] \simeq +0.2$ in the mean. Such spatial inhomogeneities could be due to recent SNe events.

Yong et al. (2006) have made an interesting study of 24 Cepheids in the outer Galactic disk based on high-resolution spectra. The distance range is $12 < R_G < 18$ kpc. Most of the Cepheids continue the trend with galactocentric distance exhibited by the Luck et al. (2006) sample, but a minority of six Cepheids have [Fe/H] around -0.8 dex and enhanced α-element abundances, $[\alpha/\mathrm{Fe}] \sim +0.3$. Thus, there is some evidence for two populations of Cepheids in the outer disk.

Cepheids can only provide information about 'present-day' gradients in the disk. Abundances of stars in open clusters may, however, be used to determine gradients at different ages. In this connection one benefits from the quite accurate ages and distances that can be determined from colour-magnitude diagrams of open clusters. For a review of results from clusters, the reader is referred to the chapter on open clusters by Friel (this volume).

5 The Galactic bulge

Due to a large distance and a high degree of interstellar absorption and reddening, the Galactic bulge is the least well known component of the Milky Way. It has been much discussed if the bulge contains only very old stars or if it also includes a younger population. This problem is related to two different scenarios for the formation of the bulge, a 'classical' bulge formed rapidly by the coalescence of star-forming clumps as suggested from the simulations of Elmegreen et al. (2008) or a 'pseudobulge' formed over a longer time through dynamical instabilities in the Galactic disk (see review by Kormendy & Kennicutt 2004). The measurement of abundance ratios in bulge stars may help to decide between these scenarios by providing information on the time-scale for the formation of the bulge.

The metallicity distribution of bulge stars has been debated for a long time. With the determination of [Fe/H] for 800 bulge giants based on VLT multi-fiber spectra with a resolution of $R \sim 20\,000$ (Zoccali et al. 2008) a robust result seems to have been obtained. Zoccali et al. observed stars in four fields having distances from the Galactic center ranging from 600 to 1600 pc. The overall metallicity distribution is centered on solar metallicity and extends from [Fe/H] $\simeq -1.5$ to $+0.5$, but with few stars in the range $-1.5 < $ [Fe/H] < -1.0. A decrease of the mean metallicity along the bulge minor axis is suggested corresponding to a gradient of ~ 0.6 dex per kpc.

A pioneering study of α/Fe ratios in 12 bulge red giants was carried out by McWilliam & Rich (1994) based on 4-meter telescope optical echelle spectra with a resolution of $R \sim 20\,000$ and typical $S/N \sim 50$. Enhanced values of [Mg/Fe] and [Ti/Fe] ($\sim +0.3$ dex) were found for all stars up to a metallicity of $\sim +0.4$ dex suggesting a very rapid formation of the bulge. In contrast, [Si/Fe] and [Ca/Fe] showed solar values, which is difficult to understand. These data are now superseeded by higher resolution spectra obtained with 8-meter class telescopes both in the optical and the infrared spectral region.

Lecureur et al. (2007) used VLT/UVES spectra in the spectral region 4800 - 6800 Å to derive O and Mg abundances relative to Fe for about 50 red bulge giants. They find that the [O/Fe] and [Mg/Fe] trends are more enhanced than the corresponding trends for thick-disk stars as determined by Bensby et al. (2005) for dwarf stars. The same conclusion is reached by Fulbright et al. (2007) from abundance ratios derived for 27 red giants observed at high resolution in the 5000 - 8000 Å spectral region with the Keck/HIRES spectrograph.

In contrast to these results, Meléndez et al. (2008) find the same [O/Fe] - [Fe/H] trend for 19 red giants belonging to the bulge and 21 thick-disk giants in the solar neighbourhood. For both samples, the oxygen and iron abundances are based on spectrum synthesis of OH and Fe I lines in an infrared spectral region around 1.55 μm as observed with Gemini/Phoenix. Hence, the comparison of the bulge and the thick disk is done in a differential way for the same type of stars. Meléndez et al. suggest that the comparisons of bulge
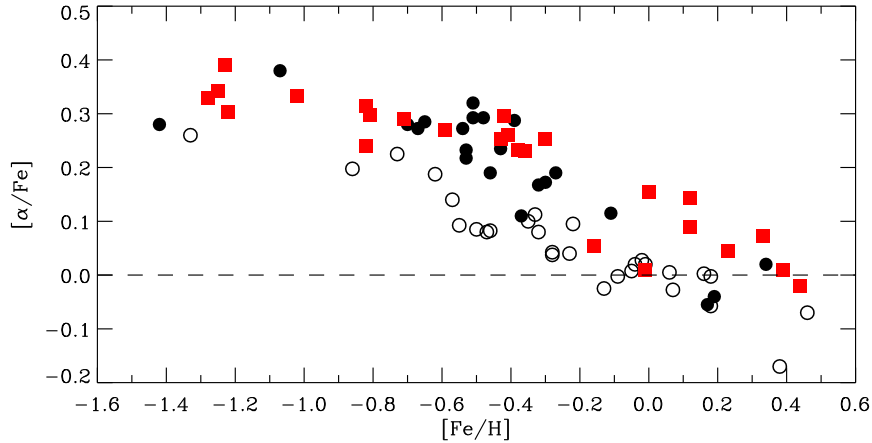
Fig. 10. The [α/Fe] - [Fe/H] relation for bulge K giant stars shown with filled (red) squares in comparison with K giants in the solar neighbourhood having either thick-disk kinematics (filled circles) or thin-disk kinematics (open circles). Data for [Mg/Fe], [Si/Fe], [Ca/Fe], and [Ti/Fe] are adopted from Alves-Brito et al. (2010).

giants with thick-disk dwarfs has led to a spurious offset of the two [O/Fe] - [Fe/H] trends due to systematic errors in the abundance ratios. When LTE is assumed and classical 1D model atmospheres are adopted, systematic errors could arise due to different non-LTE and 3D corrections for dwarf and giant stars. Recently, Ryde et al. (2010) have confirmed the results of Meléndez et al. (2008) from VLT/CRIRES high-resolution spectra of 11 red giants in the bulge.

Further evidence for an agreement between bulge and local thick-disk stars has been obtained by Alves-Brito et al. (2010) from optical high-resolution spectra. Their results are shown if Fig. 10. As seen the trends for bulge and thick-disk stars agree well with no significant differences below solar metallicity. The thin-disk stars, on the other hand, fall below the bulge and the thick disk stars. Above solar metallicity, the bulge stars tend to have higher [α/Fe] values than the disk stars but this needs to be confirmed for a larger sample.

Independent and very interesting data for abundances in the Galactic bulge have been obtained from spectra of microlensed main-sequence and subgiant stars. During a microlensing event, the flux from a star can be enhanced by a factor of 100 or even more; hence, the magnitude of a typical bulge turnoff star raises from $V \sim 18$ to $V \sim 13$. This makes it possible to obtain high-resolution spectra with good S/N. Bensby et al. (2011) have presented a homogeneous abundance study of 26 such microlensed stars using the same methods as applied for local thick-disk dwarf stars (Bensby et al. 2005). As seen from Fig. 16, there is a tendency that these microlensed bulge

stars are separated into two regions in the $[\alpha/\text{Fe}]$ – $[\text{Fe/H}]$ plane: A metal-poor group with $[\text{Fe/H}] < -0.3$ and $[\alpha/\text{Fe}] \simeq +0.3$ like the thick-disk stars, and a metal-rich group with $+0.1 < [\text{Fe/H}] < +0.6$ for which the majority of stars have $[\alpha/\text{Fe}] \simeq 0$ like the thin-disk stars, but four stars have $[\alpha/\text{Fe}] \simeq +0.1$.

Another interesting aspect of the study of microlensed main-sequence and subgiant stars is the possibility to derive ages by comparing their position in a $\log g$ - $\log T_{\text{eff}}$ diagram with isochrones computed from stellar models. According to Bensby et al. (2011) the metal-poor bulge stars have an average age of 11.2 Gyr with a dispersion of ± 2.9 Gyr much of which may be due errors in the age determination. The metal-rich bulge stars are on average younger (7.6 Gyr) and has a larger age dispersion (± 3.9 Gyr).

On the basis of these new data, Bensby et al. (2011) suggest that the bulge consists of two stellar populations, i.e. a metal-poor population similar to the thick disk in terms of metallicity range, $[\alpha/\text{Fe}]$, and age, and a metal-rich population, which could be related to the inner thin disk. Supporting evidence has recently been obtained by Hill et al. (2011) from a study of 219 red giants in Baade's bulge window (situated about four degrees from the Galactic center). $[\text{Fe/H}]$ and $[\text{Mg/Fe}]$ are derived from ESO VLT FLAMES spectra with a resoltion of $R = 20\,000$. The distribution of $[\text{Fe/H}]$ is asymmetric and can be deconvolved into two Gaussian components: a metal-poor population centred at $[\text{Fe/H}] = -0.30$ having a dispersion of 0.25 dex in $[\text{Fe/H}]$, and a metal-rich population centred at $[\text{Fe/H}] = +0.32$ with a dispersion of 0.11 dex only. The metal-poor population has $[\text{Mg/Fe}] \simeq 0.3$, whereas the stars in the metal-rich population distribute around the solar Mg/Fe ratio. These data agree well with those of Bensby et al. (2011). However, a larger set of data for microlensed bulge stars and information about chemical abundances of inner disk stars are needed before one can draw any robust conclusions about the existence of two bulge populations and the consequences this may have for models of the formation of the bulge.

6 The Galactic halo

6.1 Evidence of two distinct halo populations

For a long time, it has been discussed if the Galactic halo consists of more than one population. The classical monolithic collapse model of Eggen, Lynden-Bell & Sandage (1962) corresponds to a single halo population, but from a study of globular clusters, Searle and Zinn (1978) suggested that the halo comprises two populations: i) an inner, old, flattened population with a slight prograde rotation formed during a dissipative collapse, and ii) an outer, younger, spherical population accreted from satellite systems. This dichotomy of the Galactic halo has found support in a study of $\sim 20\,000$ stars from the Sloan Digital Sky Survey (SDSS) by Carollo et al. (2007). They find that the

inner halo consists of stars with a peak metallicity at $[\mathrm{Fe/H}] \simeq -1.6$, whereas the outer halo stars distribute around $[\mathrm{Fe/H}] \simeq -2.2$.

Several studies suggest that there is a difference in $[\alpha/\mathrm{Fe}]$ between stars that can be associated with the inner and the outer halo, respectively. Fulbright (2002) shows that stars with large values of the total space velocity relative to the LSR, $V_{\mathrm{tot}} > 300 \, \mathrm{km \, s^{-1}}$, tend to have lower values of $[\alpha/\mathrm{Fe}]$ than stars with $150 < V_{\mathrm{tot}} < 300 \, \mathrm{km \, s^{-1}}$, and Stephens & Boesgaard (2002) find that $[\alpha/\mathrm{Fe}]$ is correlated with the apo-galactic orbital distance in the sense that the outermost stars have the lowest values of $[\alpha/\mathrm{Fe}]$. Further support for such differences in $[\alpha/\mathrm{Fe}]$ comes from a study by Gratton et al. (2003), who divided stars in the solar neighbourhood into two populations according to their kinematics: i) a 'dissipative' component, which includes thick-disk stars and prograde rotating halo stars, and ii) an 'accretion' component that consists of retrograde rotating halo stars. The 'accretion' component has smaller values and a larger scatter for $[\alpha/\mathrm{Fe}]$ than the 'dissipative' component.

The differences in $[\alpha/\mathrm{Fe}]$ found in these works are not larger than about 0.1 dex, and it is unclear, if the distribution of $[\alpha/\mathrm{Fe}]$ is continuous or bimodal. Nissen & Schuster (1997) found a more clear dichotomy in $[\alpha/\mathrm{Fe}]$ for 13 halo stars with $-1.3 < [\mathrm{Fe/H}] < -0.5$. Eight of these halo stars have $[\alpha/\mathrm{Fe}]$ in the range 0.1 to 0.2 dex, whereas $[\alpha/\mathrm{Fe}] \simeq 0.3$ for the other five halo stars. Interestingly, the low-α halo stars tend to have larger apo-galactic distances than the high-α stars.

A more extensive study of 'metal-rich' halo stars has been carried out by Nissen & Schuster (2010). Stars are selected from the Schuster et al. (2006) $uvby$-β catalogue of high-velocity and metal-poor stars. To ensure that a star has a high probability of belonging to the halo population, the total space velocity with respect to the LSR is required to be larger than $180 \, \mathrm{km \, s^{-1}}$. Furthermore, Strömgren photometric indices are used to select dwarfs and subgiants with $5200 < T_{\mathrm{eff}} < 6300 \, \mathrm{K}$ and $[\mathrm{Fe/H}] > -1.6$. High-resolution, high S/N spectra were obtained with the ESO VLT/UVES and the Nordic Optical Telescope FIES spectrographs for 78 of these stars. The large majority of the stars are brighter than $V = 11.1$ and situated within a distance of 250 pc. These spectra are used to derive high-precision LTE abundance ratios in a differential analysis that also includes 16 stars with thick-disk kinematics. The precision of the various abundance ratios range from 0.02 to 0.04 dex.

Figure 11 (top) shows the distribution of $[\mathrm{Mg/Fe}]$ as a function of $[\mathrm{Fe/H}]$ for stars in Nissen & Schuster (2010). As seen, the halo stars split into two distinct populations: 'high-α' stars with a nearly constant $[\mathrm{Mg/Fe}]$ and 'low-α' stars with declining values of $[\mathrm{Mg/Fe}]$ as a function of increasing metallicity. A classification into these two populations has been done on the basis of $[\mathrm{Mg/Fe}]$, but as seen from the bottom part of the figure, $[\alpha/\mathrm{Fe}]$ would have led to the same division of the halo stars except at the lowest metallicities,
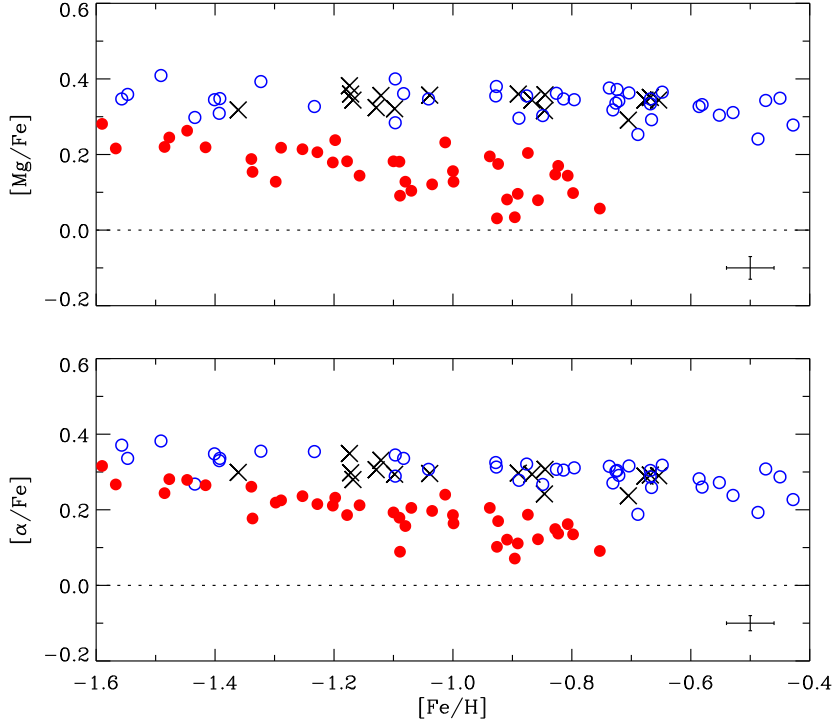
Fig. 11. [Mg/Fe] and [α/Fe] versus [Fe/H] based on data from Nissen & Schuster (2010). Stars with thick-disk kinematics are indicated by crosses and halo stars by circles. On the basis of the [Mg/Fe] distribution, the halo stars are divided into low-α stars shown by filled (red) circles, and high-α stars shown by open (blue) circles.

$-1.6 <$ [Fe/H] < -1.4, where the two populations tend to merge, and the classification is less clear.

As seen from Fig. 11, the separation in [Mg/Fe] for the two halo populations is significantly larger than the separation in [α/Fe]. At [Fe/H] $\simeq -0.8$ the mean difference in [Mg/Fe] is about 0.25 dex, whereas it is only about 0.15 dex in [α/Fe]. This is probably caused by different degrees of SNe Ia contribution to the production of Mg, Si, Ca, and Ti. According to Tsujimoto et al. (1995, Table 3), the relative contribution of SNe Ia to the solar composition is negligible for Mg, 17% for Si and 25% for Ca (Ti was not included). For comparison, the SNe Ia contribution is 57% for Fe. Hence, [Mg/Fe] is a more sensitive measure of the ratio between type II and type Ia contributions to the chemical enrichment of matter than [α/Fe]. On the other hand, it is possible to measure [α/Fe] with a higher precision than [Mg/Fe], because many more spectral lines can be used to determine [α/Fe].
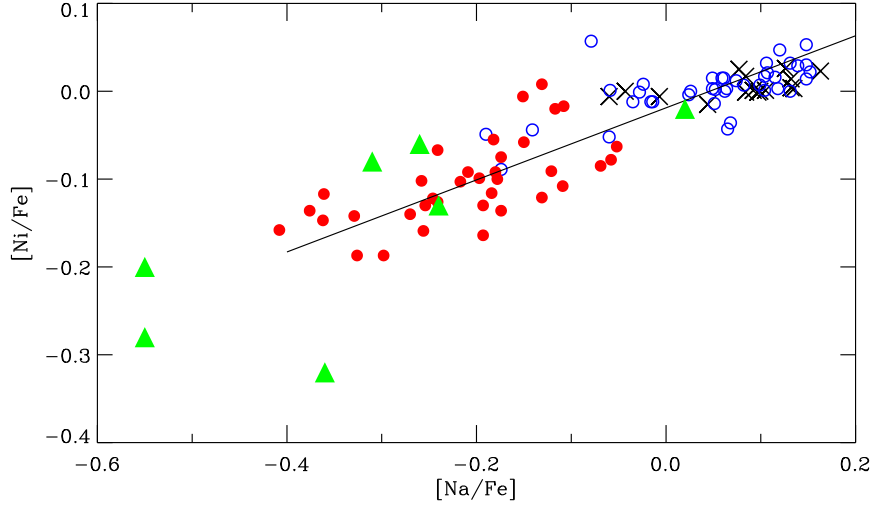
Fig. 12. The relation between [Ni/Fe] and [Na/Fe]. Local main-sequence stars from Nissen & Schuster (2010) are indicated by the same symbols as in Fig. 11, whereas the (green) triangles refer to K giants in dSph satellite galaxies from Venn et al. (2004). For both sets of data, the stars are confined to the metallicity range $-1.6 < $ [Fe/H] < -0.4.

The low-α halo stars also have low values of [Na/Fe] and [Ni/Fe] relative to the high-α stars, and as shown in Fig. 12, the two populations are well separated in a [Ni/Fe] - [Na/Fe] diagram. As seen, some stars in dSph galaxies are even more extreme in [Na/Fe] and [Ni/Fe] than the low-α halo stars.

6.2 Kinematics and origin of the two halo populations

The distribution of [α/Fe] in Fig. 11 can be explained, if the high-α stars have been formed in regions with such a high rate of chemical evolution that only type II SNe have contributed to the chemical enrichment up to [Fe/H] ~ -0.4. The low-α stars, on the other hand, originate from regions with a relatively slow chemical evolution so that type Ia SNe have started to contribute iron around [Fe/H] $= -1.6$ causing [α/Fe] to decrease towards higher metallicities until [Fe/H] ~ -0.8.

Further insight into the origin of the two halo populations can be obtained from kinematics. As seen from the Toomre energy diagram in Fig. 13, the high-α stars show evidence for being more bound to the Galaxy and favoring prograde Galactic orbits, while the low-α stars are less bound with two-thirds of them being on retrograde orbits. This suggests that the high-α population is connected to a dissipative component of the Galaxy, while the low-α stars have been accreted from dwarf galaxies.
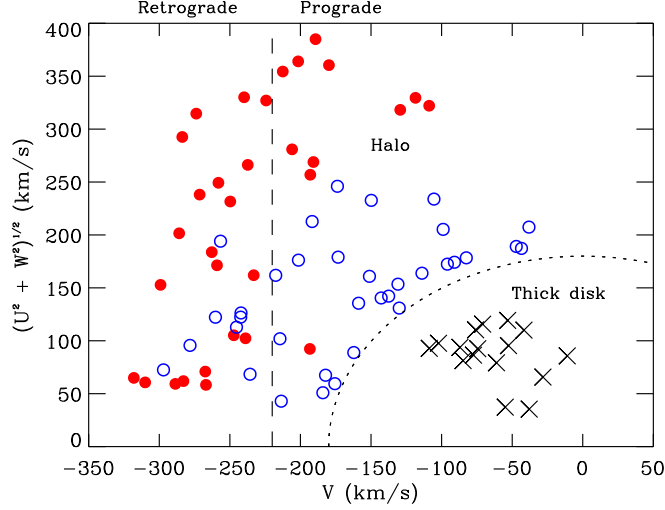
Fig. 13. Toomre diagram for stars from Nissen & Schuster (2010) having [Fe/H] $>$ -1.4. The same symbols for high-α halo, low-α halo and thick-disk stars as in Fig. 11 are used. The short-dashed circle corresponds to $V_{\text{tot}} = 180$ km s^{-1}. The long-dashed line indicates zero rotation in the Galaxy and therefore separates retrograde moving stars from prograde moving.

Several retrograde moving low-α stars have a Galactic V-velocity compo-nent similar to that of the ω Cen globular cluster, i.e. $V \sim -260$ km s^{-1}. As often discussed (e.g. Bekki & Freeman 2003), ω Cen is probably the nucleus of a captured satellite galaxy with its own chemical enrichment history. Meza et al. (2005) have simulated the orbital characteristics of the tidal debris of such a satellite dragged into the Galactic plane by dynamical friction. The captured stars are predicted to have rather small W-velocities but a wide, double-peaked U-distribution. As shown in Fig. 14, the W-U distribution ob-served for the low-α halo corresponds quite well to that prediction. There are two groups of low-α stars with $U > 200$ km s^{-1} and $U < -200$ km s^{-1}, respec-tively, corresponding to stars moving in and out of the solar neighbourhood on elongated radial orbits. Thus, a good fraction of the low-α stars, although not all, may well have originated in the ω Cen progenitor galaxy. The high-α stars, on the other hand, are confined to a much smaller range in U, i.e. from about -200 to about $+200$ km s^{-1}.

The [α/Fe] vs. [Fe/H] trend for the low-α stars in Fig. 11 and the Ni-Na trend in Fig. 12 resemble the corresponding trends for stars in dwarf galaxies. Stars in these systems tend, however, to have lower values of [α/Fe], [Na/Fe] and [Ni/Fe] than low-α halo stars. This offset agrees with simulations of the chemical evolution of a hierarchically formed stellar halo in a ΛCDM Universe by Font et al. (2006, Fig. 9). The bulk of halo stars originate from
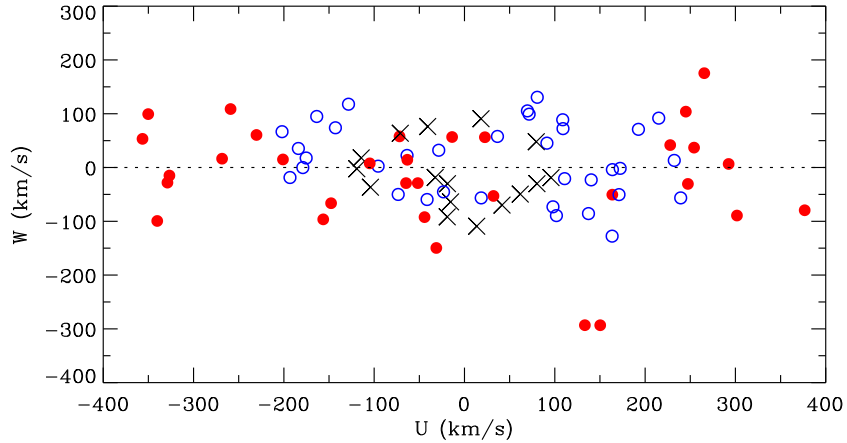
Fig. 14. The relation between the U and W velocity components for stars from Nissen & Schuster (2010) having [Fe/H] > -1.4.

early accreted, massive dwarf galaxies with efficient star formation, whereas surviving satellite galaxies in the outer halo on average have smaller masses and a slower chemical evolution with a larger contribution from Type Ia SNe at a given metallicity. The [Mg/Fe] vs. [Fe/H] trend for field stars, predicted by Font et al., agrees in fact remarkably well with the trend for the low-α halo stars.

The simulations of Font et al (2006) do not explain the existence of high-α halo stars. Two recent ΛCDM simulations suggest, however, a dual origin of stars in the inner Galactic halo. Purcell et al. (2010) propose that ancient stars formed in the Galactic disk can be ejected to the halo by merging satellite galaxies, and Zolotov et al. (2009, 2010) find that stars formed out of accreted gas in the inner 1 kpc of the Galaxy can be displaced into the halo through a succession of mergers. Alternatively, the high-α population may simply belong to the high-velocity tail of a thick disk with a non-Gaussian velocity distribution.

6.3 Globular clusters and dwarf galaxies

The Galactic halo contains more than 100 globular clusters and a number of dwarf spheroidal galaxies that are considered as Milky Way satellite systems. A dSph galaxy has a broad range in age and metallicity, whereas a globular cluster is a smaller system with a more limited range in these parameters . As often discussed, it is possible that some or all field halo stars come from dissolved globular clusters or have been accreted from previous generations of satellite galaxies. In this connection, it is is of great interest to compare the chemical abundance ratios in field stars with the corresponding ratios in still existing globular clusters and dwarf galaxies.

Globular cluster were for a long time considered as examples of systems containing a single population of stars with a well defined age and chemical composition. During the last decades it has, however, become more and more clear that many, if not all, globular clusters contain multiple stellar populations. Strong evidence comes from abundance ratios between elements from oxygen to aluminum. As reviewed by Gratton et al. (2004), high-resolution spectroscopy of red giants has revealed anti-correlations between [Na/Fe] and [O/Fe] and between [Al/Fe] and [Mg/Fe] in intermediate metallicity globular clusters. An example is shown in Fig. 15 for K giants in NGC 6752 (Yong et al. 2005).
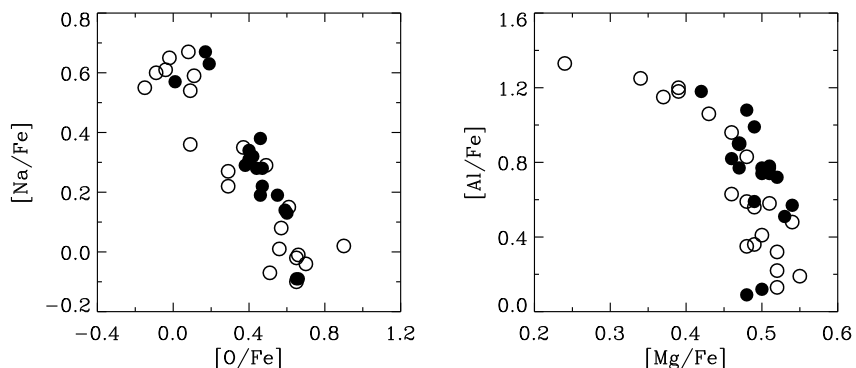
Fig. 15. The Na-O and Al-Mg anti-correlations in the globular cluster NGC 6752 based on data from Yong et al. (2005). Filled circles indicate stars near the bright end of the red-giant branch; open circles refer to less luminous stars around the red-giant bump.

The extensive study of Carretta et al. (2009) based on high-resolution VLT/UVES spectra for giant stars in 19 globular clusters indicates the existence of a [Na/Fe] - [O/Fe] anti-correlation in all cases, but the amplitude of the variations is different from cluster to cluster. Variations in [Al/Fe] correlated with [Na/Fe] are seen in the majority of clusters and an anti-correlation between [Al/Fe] and [Mg/Fe] is detected in a few cases. In addition, Yong et al. (2003) have revealed a correlation between the heavy magnesium isotope ^{26}Mg and Al in NGC 6752 by determining Mg isotope ratios from the profiles of MgH lines near 5140 Å.

All of these abundance variations are ascribed to hydrogen burning via the CNO-cycle and the NeNa and MgAl chains. Some years ago, it was much discussed if the variations were due to nuclear processes and non-standard mixing in the stars themselves or to an early generation of stars that have polluted the gas out of which the present low-mass stars in the clusters have formed. The fact that the abundance variations are not correlated with the

luminosity of the giant stars speaks against the first possibility, and when Gratton et al. (2001) discovered that a Na-O anti-correlation is present in turnoff and subgiant stars in NGC 6397 and NGC 6752, the internal mixing case was ruled out. Hence, the abundance variations must be due to an early generation of stars. Candidates are intermediate-mass AGB stars undergoing hot bottom burning (Ventura et al. 2001) and massive rotating stars (De-cressin et al. 2007).

In addition to the abundance variations of elements from O to Al, there is also increasing evidence for variations of Ca, Fe and s-process elements in several globular clusters. The classical example is ω Cen for which giant stars are found to have metallicities from $[Fe/H] \simeq -1.9$ to $\simeq -0.5$ (see review by Gratton et al. 2004). Multiple sequences in colour-magnitude diagrams are present suggesting the existence of four or five discrete populations in ω Cen with significant age and abundance differences. The more metal-rich stars in ω Cen have unusually low values of $[Cu/Fe]$ (Cunha et al. 2002) and very high values of the abundances of the second-peak s-process elements, i.e. $[Ba/Fe]$ and $[La/Fe]$ values around 1.0 dex (Smith et al. 2000). These abundance anomalies point to a complicated chemical evolution history, in which ω Cen was originally the nucleus of a much larger dwarf galaxy that merged with the early Galactic disk (Bekki & Freeman 2003).

Evidence for abundance variations of Ca, Fe, and s-process elements has been found for other clusters than ω Cen. On the basis of high-resolution spectroscopy with UVES of eight giant stars in NGC 1851, Yong & Grundahl (2008) found a range of 0.6 dex in $[Zr/Fe]$ and $[La/Fe]$, and Marino et al. (2009) found similar large variations in $[Y/Fe]$, $[Zr/Fe]$ and $[Ba/Fe]$ for 17 giant stars in M 22. In addition, there is a correlation between these ratios and $[Fe/H]$, which varies from -1.9 to -1.5 in M 22. Evidence of variations in $[Ca/Fe]$ is also found in other globular clusters by Lee et al. (2009) from photometric measurements of an index of the Ca II H and K lines, but Car-retta et al. (2010) do not confirm this on the basis of high-resolution UVES spectra. Instead, they suggest that the spread in the Ca II H and K index may be related to variations in helium and nitrogen abundances.

Some authors, e.g. Lee et al. (2009), suggest that all globular clusters were once nuclei of dwarf galaxies that are now accreted and dissolved in the Milky Way. In this connection, one may wonder why practically no field halo stars share the Na-O abundance anomalies of the globular clusters. Perhaps the explanation is that the elements produced by AGB stars are confined to the potential wells of the clusters. According to the hydrodynamical simulations by D'Ercole et al. (2008), the gas ejected by AGB stars collects in cooling flows into the cores of globular clusters.

The chemical composition of giant stars in dSph galaxies is reviewed by Tolstoy et al. (2009). For the large majority of stars with $[Fe/H] > -2$, $[\alpha/Fe]$ is significantly lower than in halo and disk stars belonging to the Milky Way. Two examples are shown in Fig. 16. Stars in Sculptor (Kirby et al. 2009)
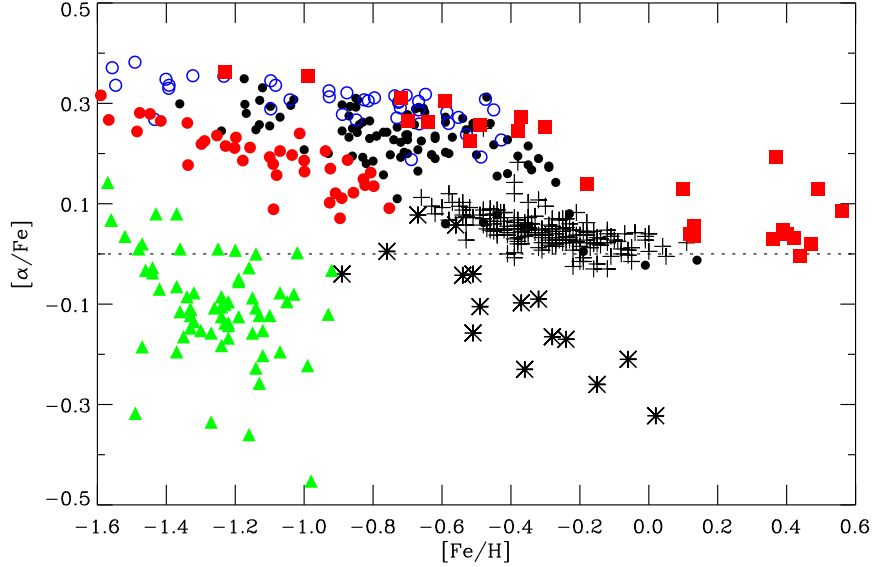
Fig. 16. $[\alpha/\mathrm{Fe}]$ vs. $[\mathrm{Fe/H}]$ for various stellar populations. Thin-disk stars from Reddy et al. (2003) are shown with plus symbols. Filled circles refer to thick-disk stars from Reddy et al. (2006) and Nissen & Schuster (2010). Filled (red) squares are microlensed bulge stars from Bensby et al. (2011). Open (blue) circles are high-α and filled (red) circles low-α halo stars from Nissen & Schuster (2010). Asterisks refer to stars in the Sagittarius dSph galaxy (Sbordone et al. 2007), and filled (green) triangles show data for stars in the Sculptor dSph galaxy from Kirby et al. (2009) for which the precision of $[\alpha/\mathrm{Fe}]$ is better than 0.15 dex.

distribute around $[\alpha/\mathrm{Fe}] = -0.1$, and do not seem to have metallicities above $[\mathrm{Fe/H}] \sim -0.9$. The other example is the Sagittarius dwarf galaxy, which was discovered by Ibata et al. (1994) to be merging with the Milky Way. The abundances derived by Sbordone et al. (2007) for giant stars show a declining trend of $[\alpha/\mathrm{Fe}]$ reaching $[\alpha/\mathrm{Fe}]$ as low as -0.3 dex at solar metallicity.

Evidently, present day dSph galaxies have had a chemical evolution history different from that of the other main components of the Milky Way. In addition to the underabundance of $[\alpha/\mathrm{Fe}]$, the more metal-rich stars in dSph galaxies stand out by having low $[\mathrm{Na/Fe}]$ and $[\mathrm{Ni/Fe}]$ abundances (Fig. 11) as well as high $[\mathrm{Ba/Y}]$ ratios (Venn et al. 2004). At the lowest metallicities, $[\mathrm{Fe/H}] < -2$, the abundance ratios are, however, similar to those in Galactic halo stars, which suggests that the abundance deviations of dSph stars should not be explained in terms of an anomalous IMF. The most obvious reason for the underabundances of $[\alpha/\mathrm{Fe}]$ is that the star formation rate in surviving dSph galaxies has been so slow that type Ia SNe started to contribute Fe at a metallicity of $[\mathrm{Fe/H}] \sim -2$. Dwarf galaxies are, however, not ruled out as

'building blocks' of the Galactic halo, because early accreted dSph galaxies probably have had a somewhat faster chemical evolution than the less masive present-day dSph galaxies in the outer halo (Font et al. 2006).

7 Conclusions

The last decade has seen great progress in determinations of abundance ratios that can be used as tracers of stellar populations. This has been possible due to the availability of high-resolution echelle spectrographs at large telescopes – in some cases with multiplex capabilities so that many stars, e.g. in clusters and dwarf galaxies, can be observed simultaneously. Determinations of $[\alpha/\text{Fe}]$ from low- or medium-resolution spectroscopy, e.g. in the SDSS and RAVE surveys, are also important in connection with large statistical investigations of stellar populations. Similar measurements of $[\alpha/\text{Fe}]$ will be obtained in connection with the GAIA mission. Furthermore, abundances of Galactic bulge stars are now been obtained from high-resolution infrared spectra, but the spectral coverage is small and there is no multiplex advantages. Hence, the number of bulge stars studied with infrared spectra is still limited. More efficient infrared echelle spectrographs with multiplex capabilities are needed to take advantage of the lower reddening in the infrared spectral region, when dealing with the bulge and the inner part of the disk.

Elemental abundance ratios are derived by the aid of a model atmosphere analysis of the available stellar spectra as discussed in Sect. 2. Most studies are still based on homogeneous model atmospheres and the assumption of LTE, but several works show that inhomogeneous models and deviations from LTE can change the derived abundances significantly. Such 3D and non-LTE modelling is difficult to carry out and in some cases the derived abundances are sensitive to uncertain hydrogen collision cross sections. Hence, the derived trends of abundance ratios as a function of metallicity can be quite uncertain. On the other hand, it is possible to determine precise differences of abundance ratios by a 1D LTE analysis of a sample of stars confined to small ranges in effective temperature, surface gravity and metallicity. In this way, abundance ratios can be used to disentangle stellar populations. Care should, however, be taken when comparing different spectral types and luminosity classes, such as F and G dwarfs with K giants, because systematic errors may be important.

As discussed in Sect. 3, the abundance ratios $[\alpha/\text{Fe}]$, $[\text{C/O}]$, $[\text{Na/Fe}]$, $[\text{Ni/Fe}]$, $[\text{Cu/Fe}]$, $[\text{Eu/Ba}]$, and $[\text{Ba/Y}]$ are of high interest as tracers of stellar populations. The usefulness of these ratios is related to the fact that the elements involved are produced in different types of stars. The nucleosynthesis is not well understood for all elements, but it seems that variations of the ratios from one population to the next can be explained in terms of different rates of star formation and chemical evolution. In general, one does not need to invoke variations in the initial mass function to explain the abundance

ratios. A better understanding of the nucleosynthesis of the elements is, however, important in order to learn more about the formation and evolution of the various populations.

The power of abundance ratios as population tracers is evident from Fig. 16, where $[\alpha/\text{Fe}]$ is plotted as a function of $[\text{Fe/H}]$ for seven different populations. $[\alpha/\text{Fe}]$ is defined as the average value of $[\text{Mg/Fe}]$, $[\text{Si/Fe}]$, $[\text{Ca/Fe}]$ and $[\text{Ti/Fe}]$, and may be used to estimate the time-scale for the chemical enrichment of the population, as explained in Sect. 3.2. On the basis of this figure and the more detailed discussion in the previous sections, the following conclusions about stellar populations in the Galactic disk, the bulge and the halo can be made.

The disk consists of two main populations, the thin and the thick disk, which differ in $[\alpha/\text{Fe}]$ as well as $[\text{C/O}]$ and $[\text{Eu/Ba}]$. The thick disk is formed on a relatively short time-scale with enrichment from type II SNe only up to $[\text{Fe/H}] \simeq -0.4$. Thin-disk stars have lower values of $[\alpha/\text{Fe}]$ due to type Ia SNe contributions to the chemical enrichment; hence the time-scale of evolution is longer than in the case of the thick disk. In the metallicity range $-0.7 < [\text{Fe/H}] < -0.4$, a gap in $[\alpha/\text{Fe}]$ is present between the two disks. Altogether, the $[\alpha/\text{Fe}]$ distribution of disk stars is well explained by a scenario, for which a period of rapid star formation in the early Galactic disk was interrupted by a merging satellite galaxy that 'heated' the already formed stars to thick-disk kinematics. This was followed by a hiatus in star formation, in which metal-poor gas was accreted and type Ia SNe caused $[\alpha/\text{Fe}]$ to decrease. When star formation resumed, the first thin disk stars formed with low metallicity and low $[\alpha/\text{Fe}]$. However, as discussed in Sect. 4.2, an alternative model with a monotonically decreasing star formation rate and radial migration of stars and gas (Schönrich & Binney 2009a, 2009b) also predicts a bimodal distribution of $[\alpha/\text{Fe}]$. Very precise measurements of the distributions of $[\alpha/\text{Fe}]$ as well as $[\text{C/O}]$ and $[\text{Eu/Ba}]$ for a large volume-limited sample of F and G main-sequence stars would be important to distinguish between the two competing models for disk formation.

For the bulge, there has been great progress in studies of abundance ratios in recent years. In some works, enhanced values of $[\alpha/\text{Fe}] \sim +0.3$ are found for stars as metal-rich as the Sun, but in the most precise differential studies (Alves-Brito et al. 2010), the trend of $[\alpha/\text{Fe}]$ for the bulge is found to be similar to that of the thick disk (Fig. 10). The abundances derived by Bensby et al. (2011) for microlensed main-sequence stars (Fig. 16) suggest that the bulge may consist of two distinct populations: i.e. old metal-poor stars with enhanced $[\alpha/\text{Fe}]$ ratios related to the thick disk, and younger very metal-rich stars with disk-like α/Fe ratios. Still, one would like to see many more bulge stars observed before drawing conclusions concerning models for bulge formation from the abundance ratios.

For halo stars in the solar neighbourhood, there is evidence for the existence of two distinct populations clearly separated in $[\alpha/\text{Fe}]$, $[\text{Na/Fe}]$ and

[Ni/Fe] as discussed in Sect. 6.1. The high-α stars have abundance ratios very similar to thick-disk stars. They may be ancient stars formed in the Galactic disk or bulge and ejected to the halo by merging satellite galaxies (Purcell et al. 2010; Zolotov et al. 2009, 2010), or they may simply belong to the high-velocity tail of a thick disk with a non-Gaussian velocity distribution. The low-α stars tend to have retrograde motions and many of them move on elongated radial orbits close to the Galactic plane as predicted for the stellar debris of the captured ω Cen progenitor galaxy. It is likely that the low-alpha stars have been accreted from dSph galaxies with a relatively slow chemical evolution, for which type Ia SNe started to contribute iron at [Fe/H] ~ -1.5. Perhaps future precise studies of abundance ratios of larger samples of halo stars will reveal additional subpopulations.

Stars in surviving dSph galaxies have even lower values of [α/Fe] than the low-α halo stars as seen from Fig. 16. This is to be expected according to simulations of the chemical evolution of a hierarchically formed stellar halo in a ΛCDM Universe (Font et al. 2006). Present day dSph galaxies in the outer halo have experienced a slower chemical evolution than more massive satellite galaxies accreted in the early Galxy.

All globular clusters seem to consist of multiple stellar populations characterized by different values of [O/Fe], [Na/Fe], [Al/Fe], and [Mg/Fe]. This may be due to chemical enrichment from intermediate-mass AGB stars undergoing hot-bottom hydrogen burning. There is also evidence for variations of [Fe/H] and the abundance of s-process elements in several globular clusters, most notable in ω Cen. In this connection, it has been suggested that globular clusters were once the nuclei of now dissolved dwarf galaxies.

Precise abundance ratios of field stars belonging to the Galactic halo have so far only been obtained in a small region around the Sun. It would be important to extend such studies to more distant halo regions. To do this in an efficient way one needs a fiber-coupled high-resolution spectrograph that would make it possible to observe many stars simultaneously over a relatively large field, say one degree in diameter. Such a spectrograph would also be very useful in exploring abundance gradients in the Galactic disk, both radially and in the direction towards the Galactic poles.

References

1. Alves-Brito, A., Meléndez, J., Asplund, M., Ramírez, I., & Yong, D. 2010, A&A, 513, A35
2. Arlandini, C., Käppeler, F., Wisshak, K., et al. 1999, ApJ, 525, 886
3. Arnett, W. D. 1971, ApJ, 166, 153
4. Asplund, M. 2005, ARA&A, 43, 481
5. Asplund, M., Grevesse, N., Sauval, A.J., & Scott, P. 2009, ARA&A, 47, 481
6. Barklem, P. S., Christlieb, N., Beers, T. C., et al. 2005, A&A, 439, 129
7. Bekki, K., & Freeman, K. C. 2003, MNRAS, 346, L11

8. Bensby, T., & Feltzing, S. 2006, MNRAS, 367, 1181

9. Bensby, T., Adén, D., Melédez, J., et al. 2011, A&A, 533, A134

10. Bensby, T., Feltzing, S., Lundström, I., & Ilyin, I. 2005, A&A, 433, 185

11. Boeche, C., Siebert, A., & Steinmetz, M. 2008, AIP Conference Ser., 1082, 61

12. Bergemann, M., & Cescutti, G. 2010, A&A, 522, A9

13. Bergemann, M., & Gehren, T. 2008, A&A, 492, 823

14. Bergemann, M., Pickering, J. C., & Gehren, T. 2010, MNRAS, 401, 1334

15. Busso, M., Gallino, R., & Wasserburg, G. J. 1999, ARA&A, 37, 239

16. Carollo, D., Beers, T. C., Lee, Y. S., et al. 2007, Nature, 450, 1020

17. Carretta, E., Bragaglia, A., Gratton, R. G., & Lucatello, S. 2009, A&A, 505, 139

18. Carretta, E., Bragaglia, A., Gratton, R., et al. 2010, ApJ, 712, L21

19. Casagrande, L., Ramírez, I., Meléndez, J., Bessell, M., & Asplund, M. 2010, A&A, 512, A54

20. Cayrel, R., Depagne, E., Spite, M., et al. 2004, A&A, 416, 1117

21. Chen, Y. Q., Nissen, P. E., Zhao, G., & Asplund, A. 2002, A&A, 390, 225

22. Chen, Y. Q., Nissen, P. E., Zhao, G., Zhang, H. W., & Benoni, T. 2000, A&AS, 141, 491

23. Chiappini, C., Hirschi, R., Meynet, G., et al. 2006, A&A, 449, L27

24. Cooke, R., Pettini, M., Steidel, C.C., Rudie, G.C., & Nissen, P.E. 2011, MN-RAS (in press), arXiv:1106.2805

25. Cunha, K., Smith, V. V., Suntzeff, N. B., et al. 2002, AJ, 124, 379

26. Decressin, T., Meynet, G., Charbonnel, C., Prantzos, N., & Ekström, S. 2007, A&A, 464, 1029

27. D'Ercole, A., Vesperini, E., D'Antona, F., et al. 2008, MNRAS, 391, 825

28. Drawin, H. W. 1969, Z. Phys., 225, 483

29. Edvardsson, B., Andersen, J., Gustafsson, B., et al. 1993, A&A, 275, 101

30. Eggen, O. J., Lynden-Bell, D., & Sandage, A. R. 1962, ApJ, 136, 748

31. Elmegreen, B. G., Bournaud, F., & Elmegreen, D. M. 2008, ApJ, 688, 67

32. Fabbian, D., Nissen, P. E., Asplund, M., Pettini, M., & Akerman, C. 2009, A&A, 500, 1143

33. Fenner, Y., Gibson, B. K., Gallino, R., & Lugaro, M. 2006, ApJ, 646, 184

34. Font, A. S., Johnston, K. V., Bullock, J. S., & Robertson, B. E. 2006, ApJ, 638, 585

35. Fuhrmann, K. 2004, AN, 325, 3

36. Fulbright, J. P. 2002, AJ, 123, 404

37. Fulbright, J. P., McWilliam, A., & Rich, R. M. 2007, ApJ, 661, 1152

38. Gehren, T., Liang, Y. C., Shi, J. R., Zhang, H. W., & Zhao, G. 2004, A&A, 413, 1045

39. Gilmore, G., & Reid, N. 1983, MNRAS, 202, 1025

40. González Hernández, J. I., & Bonifacio, P. 2009, A&A, 497, 497

41. Gratton, R. G., Bonifacio, P., Bragaglia, A., et al. 2001, A&A, 369, 87

42. Gratton, R. G., Carretta, E., Desidera, S., et al. 2003, A&A, 406, 131

43. Gratton, R., Carretta, E., Matteucci, F., & Sneden, C. 1996, ASP Conf. Ser., 92, 307

44. Gratton, R. G., Sneden, S., & Carretta, E. 2004, ARA&A, 42, 385

45. Gustafsson, B., Edvardsson, B., Eriksson, K., et al. 2008, A&A, 486, 951

46. Haywood, M. 2008, MNRAS, 388, 1175

47. Hill, V., Lecureur, A., Gómez, A., et al. 2011 A&A (in press), arXiv:1107.5199

48. Ibata, R. A., Gilmore, G.,& Irwin, M. J. 1994, Nature, 370, 194
49. Israelian, G., & Rebolo, R. 2001, ApJ, 557, L43
50. Kirby, E. N., Guhathakurta, P., Bolte, M., Sneden, C., & Geha, M. C. 2009, ApJ, 705, 328
51. Kormendy, J., & Kennicutt Jr., R. C. 2004, ARA&A, 42, 603
52. Korn, A. J., Grundahl, F., Richard, O., et al. 2007, ApJ, 671, 402
53. Kurucz, R. 1993, ATLAS9 Stellar Atmosphere Programs and 2 km/s grid. Kurucz CD-ROM No. 13. Cambridge, Mass., Smithsonian Astrophysical Observatory
54. Lecureur, A., Hill, V., Zoccali, M., et al. 2007, A&A, 465, 799
55. Lee, J-W., Kang, Y-W., Lee, J., & Lee, Y-W. 2009, Nature, 462, 480
56. Lee, Y.S., Beers, T.C., An, D., et al. 2011, ApJ, 738, 187
57. Luck, R. E., Kovtyukh, V. V., & Andrievsky, S. M. 2006, AJ, 132, 902
58. Marino, A. F., Milone, A. P., Piotto, G., et al. 2009, A&A, 505, 1099
59. Mashonkina, L., Gehren, T., Shi, J.-R., Korn, A.J., & Grupp, F. 2011, A&A, 528, A87
60. Mashonkina, L., Gehren, T., Travaglio, C., & Borkova, T. 2003, A&A, 397, 275
61. McWilliam, A., Preston, G. W., Sneden, C., & Searle, L. 1995, AJ, 109, 2757
62. McWilliam, A., & Rich, R. M. 1994, ApJS, 91, 749
63. Meléndez, J., Asplund, M., Alves-Brito, A., et al. 2008, A&A, 484, L21
64. Meléndez, J., Asplund, M., Gustafsson, B., & Yong, D. 2009, ApJ, 704, L66
65. Meza, A., Navarro, J. F., Abadi, M. G., & Steinmetz, M. 2005, MNRAS, 359, 93
66. Mishenina, T. V., Kovtyukh, V. V., Soubiran, C., Travaglio, C., & Busso, M. 2002, A&A, 396, 189
67. Neves, V., Santos, N. C., Sousa, S. G., Correia, A. C. M., & Israelian, G. 2009, A&A, 497, 563
68. Nissen, P. E. 2008, Physica Scripta, T133, 014022
69. Nissen, P. E., Akerman, C., Asplund, M., et al. 2007, A&A, 469, 319
70. Nissen, P. E., Primas, F., Asplund, M., & Lambert, D. L. 2002, A&A, 390, 235
71. Nissen, P. E., & Schuster, W. J. 1997, A&A, 326, 751
72. Nissen, P. E., & Schuster, W. J. 2010, A&A, 511, L10
73. Nissen, P. E., & Schuster, W. J. 2011, A&A, 530, A15
74. Nordström, B., Mayor, M., Andersen, J., et al. 2004, A&A, 418, 989
75. Pompéia, L., Hill, V., Spite, M., et al. 2008, A&A, 480, 379
76. Purcell, C. W., Bullock, J. S., & Kazantzidis, S. 2010, MNRAS, 404, 1711
77. Ramírez, I., Allende Prieto, C., & Lambert, D. L. 2007, A&A, 465, 271
78. Reddy, B. E., Lambert, D. L., & Allende Prieto, C. 2006, MNRAS, 367, 1329
79. Reddy, B. E., Tomkin, J., Lambert, D. L., & Allende Prieto, C. 2003, MNRAS, 340, 304
80. Romano, D., & Matteucci, F. 2007, MNRAS, 378, L59
81. Ryde, N., Gustafsson, B., Edvardsson, B., et al. 2010, A&A, 509, A26
82. Sbordone, L., Bonifacio, P., Buonanno, R., et al. 2007, A&A, 465, 815
83. Schönrich, R., & Binney, J. 2009a, MNRAS, 396, 203
84. Schönrich, R., & Binney, J. 2009b, MNRAS, 399, 1145
85. Schuster, W. J., Moitinho, A., Márquez, A., Parrao, L., & Covarrubias, E. 2006, A&A, 445, 939
86. Searle, L., & Zinn, R. 1978, ApJ, 225, 357

87. Smith, V. V., Suntzeff, N. B., Cunha, K., et al. 2000, AJ, 119, 1239
88. Sousa, S. G., Santos, N. C., Israelian, G., Mayor, M., & Monteiro, M. J. P. F. G. 2007, A&A, 469, 783
89. Stephens, A., & Boesgaard, A. M. 2002, AJ, 123, 1647
90. Strömgren, B. 1987, In The Galaxy, ed. G. Gilmore & B. Carswell (Reidel, Dordrecht), 229
91. Takeda, Y., Hashimoto, O., & Taguchi, H. 2005, PASJ, 57, 751
92. Tolstoy, E., Hill, V., & Tosi, M. 2009, ARA&A, 47, 371
93. Tsujimoto, T., Nomoto, K., Yoshii, Y., et al. 1995, MNRAS, 277, 945
94. Turcotte, S., & Wimmer-Schweingruber, R. F. 2002, Journal of Geophysical Research, 107, 1442
95. Venn, K. A., Irwin, M., Shetrone, M. D., et al. 2004, AJ, 128, 1177
96. Ventura, P., D'Antona, F., Mazzitelli, I., & Gratton, R. 2001, ApJ, 550, L65
97. Yong, D., Carney, B. W., Teixera de Almeida, M. L., & Poha, B. L. 2006, AJ, 131, 2256
98. Yong, D., & Grundahl, F. 2008, ApJ, 672, L29
99. Yong, D., Grundahl, F., Lambert, D. L., Nissen, P. E., & Shetrone, M. D. 2003, A&A, 402, 985
100. Yong, D., Grundahl, F., Nissen, P. E., Jensen, H. R., & Lambert, D. L. 2005, A&A, 438, 875
101. Zoccali, M., Hill, V., Lecureur, A., et al. 2008, A&A, 486, 177
102. Zolotov, A., Willman, B., Brooks, A. M., et al. 2009, ApJ, 702, 1058
103. Zolotov, A., Willman, B., Brooks, A. M., et al. 2010, ApJ, 721, 738

List of abbreviations

AGB: Asymptotic Giant Branch
CDM: Cold Dark Matter
CRIRES: CRyogenic InfraRed Echelle Spectrograph
DEIMOS: DEep Imaging Multi-Object Spectrograph
DLA: Damped Lyman-Alpha
dSph: dwarf Spheroidal
ESA: European Space Agency
ESO: European Southern Observatory
EW: Equivalent Width
FIES: FIbre fed Echelle Spectrograph
FLAMES: Fibre Large Array Multi-Element Spectrograph
GAIA: (ESA mission for exploring the Galaxy)
HARPS: High Accuracy Radial velocity Planet Searcher
HFS: Hyper-Fine Structure
HIRES: HIgh Resolution Echelle Spectrometer
H-R: Hertzsprung-Russell
IMF: Initial Mass Function
LMC: Large Magellanic Cloud
LSR: Local Standard of Rest
LTE: Local Thermodynamic Equilibrium
NOT: Nordic Optical Telescope
RAVE: Radial Velocity Experiment
SDSS: Sloan Digital Sky Survey
SNe: Supernovae
UVES: Ultra-violet and Visible Echelle Spectrograph
VLT: Very Large Telescope

Index terms

Chemical evolution
Dwarf galaxies
Echelle spectrographs
Effective temperature
Galactic halo
Galactic disk
Galactic bulge
Globular clusters
Nucleosynthesis
Stellar atmospheres
Stellar abundances
Stellar metallicity
Stellar populations